DCPM 18/KFA 1

"Core-Management Studies"

by

B. Biele and Dr. A. Dworak

Jülich, March 1974

The aim of the here presented two studies is to investigate the possibilities of achieving an axial graduated power distribution, similar to the powershape present in a Pebbelbed-HTR with the OTTO-refueling-management. Two schemes were investigated, in Part 1, the results of the "Axial-Pushthrough" are quoted whereas in Part 2 the first results of the "Layer Loading System" (LLS) are given.

"The Axial Push-Through" Part 1

by

B. Biele

1. Introduction

The principle of the Pushthrough Fuel Management here considered for an HTR with eight rows of block-type fuel elements is to discharge the two lowest layers of fuel elements after one year, to lower the balance of the core, and to charge at the top two layers of fresh fuel elements (GGA concept). The advantages of this reload scheme are:

(a) only equal-age fuel elements are on the same level
(b) highly satisfactory axial power distribution
(c) low maximal fast dose
(d) low pressure drop in the core

However, these advantages have to be traded for complicate charge and discharge operations.

The purpose of the present investigation is summarized as follows:

1. Investigation into the neutron-physical and thermodynamic potentials of a core subjected to this type of fuel management, at the same time settling the questions whether a core with high heavy-metal content is preferable to a core with a low content.
2. Testing the possibility of additional advantages by selection of another fuel-element type after the most satisfactory core layout has been determined.

The program system VSOP has been employed to compute the fuel cycle. The core model with three radial and four axial regions is shown in Fig. 1. The temperatures were computed with the aid of a program based on extensive computations of heat transition in various variants of pressed fuel elements and on the consideration of the dependence of thermal conductivity on temperature and dose.

2. Determining the Most Satisfactory Core Layout

2.1 Layout Criteria

The reactor is operated in a one-year Th-U cycle using pressed block elements (Monolith, Fig. 2). One quarter of all fuel elements is to be replaced at the end of a cycle. The excess reactivity at the end of a cycle will still be high enough to permit a load variation of 100-40-100 %.

The axial power distribution should be selected so that the fuel centre temperature above the core height is as constant as possible, i.e. the power should decrease from top to bottom. This should be achieved by different Th and U 235 inventory in the axial regions. Moreover, the burn-up of U 235 and the building-up of U 233 should take place in equal proportions in order to achieve a power distribution that is independent of time.

Since burnable poisons and control rods are not specially taken into account, the k_{eff} was adjusted to 1.0 by boron uniformly distributed in the core.

2.2 Layout Data

Table 1 Core Data

Electric power	MW	1000
Thermal power	MW	2604
Efficiency	%	38.4
Power density	MW/m^3	8.32
Core diameter D	m	7.92
Core height H	m	6.352
H/D		0.802
Reflector thickness	m	1.2
Inlet gas temperature	^oC	460
Outlet gas temperature (mixed)	^oC	850
Bypass	%	8.0
Gas pressure in primary circuit	atm	60

Table 2 Data of the Monolith-Fuel Element (Fig. 2)

Width over flats	cm	36
Block height	cm	79.4
Pitch	cm	2.3
Cooling channel diameter	cm	1.9
Fuel channel diameter	cm	1.9
Ligament thickness	cm	0.4
Block without control rods		
Number of coolant holes		72
Number of fuel pins		138
Block with control rods		
Number of coolant holes		43
Number of fuel pins		80
Average unused space (gripping-hole, control rods, granulate, gaps between blocks)	%	6.72
Maximum thermal flow	W/cm^2	50
Graphite density	g/cm^3	1.7
Maximum fast dose	EDN	5.3 x E21
Effective graphite absorption cross-section for 0.0253 eV	mb	4.5

Table 3 Fuel Data

Fuel		UO_2 - ThO_2
Coated particle		
Breed: kernel diameter	mm	0.60
coating thickness	mm	0.16
Feed: kernel diameter	mm	0.25
coating thickness	mm	0.18
density UO_2	g/cm^3	10.5
ThO_2	g/cm^3	9.5
matrix	g/cm^3	1.7
Max. fuel centre temperature	^oC	1350
Max. burn-up	GWd/t	120

Table 4 Data of Temperature Computations

1) Thermal conductivity as function of temperature and fast dose
2) No gagging assumed

2.3 Core Layouts

2.3.1 Case A: Layout of a Core with Low Heavy-Metal Content and High Burn-up

A core layout with low content of heavy metal ensures satisfactory life performance of the pressed block elements because of the small difference between the material-data in the fuel and the graphite regions.

The initial core data are compiled in Table 5.

Table 5 Results of Core Layout (Case A)

		R1+R2		R3		R4
Z1	N_C/N_{SM}	270	Z5	255	Z8	255
	E	9.3		9.7		9.5
	FF	16.75		17.90		20.13
	SMD	0.293		0.310		0.350
Z2	N_C/N_{SM}	270	Z6	255	Z9	225
	E	9.3		9.7		9.5
	FF	16.75		17.90		20.13
	SMD	0.293		0.310		0.350
Z3	N_C/N_{SM}	255	Z7	255	Z10	255
	E	4.2		4.0		4.0
	FF	15.33		15.23		17.22
	SMD	0.310		0.310		0.350
Z4	N_C/N_{SM}	255	Z4	255	Z4	255
	E	2.5		2.5		2.5
	FF	14.53		14.53		14.53
	SMD	0.310		0.310		0.310

$\overline{N_C/N_{SM}} = 253$; $\overline{N_C/N_{TH}} = 267$

N_C/N_{SM} = ratio of mean atom densities of graphite and heavy metal

E = enrichment in per cent, referred to heavy metal

FF = volume loading, i.e. share by volume of coated particles in the fuel region

SMD = heavy metal density in the fuel region

The reload operations always involves the three fuel-element types in the regions Z1 and Z2, Z5 and Z6, Z8 and Z9. The equilibrium core is achieved after three reload operations. All further data and statements refer to the equilibrium core.

Table 6 Results of Core Layout (Core A, Equilibrium Core)

		Start	End
K_{eff}		1.315	1.015
X_e-Override (100-40-100 %)		1.017	1.013
Leakage (%)		4.35	3.82
Radial Power Formfactors	R1	0.988	0.991
	R2	0.981	0.986
	R3	0.997	1.020
	R4	1.034	1.004
Core Inventory [kg]	Th232	26843	26358
	U235	1165.3	508.3
	U233	474.3	581.3
		Charge	Discharge
Inventory in the fuel elements [kg]	Th323	7010.8	6530.6
	U235	747.5	92.98
	U233	-	161.1
Balance Δ U235 [kg]		654.5	
Average conversion ratio		0.4573	
Average Burn up (GWd/t)		99.2	
Maximum Burn up (GWd/t)		113.5	
Average fast Dose of the discharged fuel elements (10^{21} EDN)		3.14	
Maximum fast Dose		3.59	

2.3.2 Case B: Layout of a Core with High Heavy-Metal Content and Low Burn-up

The results of Case A - especially the k_{eff} vs. time - suggest that the high excess reactivity at the beginning of the cycle should be lowered by absorption in fertile material. The k_{eff} characteristic would be flatter because a substantial amount of bred U 233 can be expected.

The use of heavy metal is limited by the volume loading which is about 40 % in the compressed block.

Table 7 Results of Core Layout (Case B; first core)

		R1-R2		R3		R4
Z1	N_C/N_{SM}	185	Z5	170	Z8	150
	E	6.1		6.5		6.4
	FF	22.19		24.37		27.43
	SMD	0.424		0.460		0.520
Z2	N_C/N_{SM}	185	Z6	170	Z9	150
	E	6.1		6.5		6.4
	FF	22.19		24.37		27.43
	SMD	0.424		0.460		0.520
Z3	N_C/N_{SM}	170	Z7	170	Z10	150
	E	3.4		3.6		3.7
	FF	22.21		22.35		25.32
	SMD	0.460		0.460		0.519
Z4	N_C/N_{SM}	180	Z4	180	Z4	180
	E	2.8		2.8		2.8
	FF	20.62		20.62		20.62
	SMD	0.435		0.435		0.435

$\overline{N_C/N_{SM}} = 174.4$ $\overline{N_C/N_{TH}} = 182$

The results of the core layout for the equilibrium core achieved after three recharging processes are compiled in Table 8.

Table 8 Results of Core Layout (Case B, Equilibrium Core)

		Start	End
K_{eff}		1.176	1.011
X_e-Override (100-40-100 %)		1.015	1.010
Leakage (%)		3.83	3.40
Radial Power Formfactors	R1	1.023	1.002
	R2	0.989	0.993
	R3	0.988	1.015
	R4	1.000	0.990
Core Inventory [kg]	Th232	41287	40653
	U235	1340.7	742.0
	U233	675.3	853.9
		Charge	Discharge
Inventory in the fuel elements [kg]	Th232	10675.0	10049.0
	U235	729.0	129.5
	U233	-	245.9
Balance Δ U235 [kg]		599.5	
Average conversion ratio		0.5919	
Average Burn up (GWd/t)		68.5	
Maximum Burn up (GWd/t)		83.9	
Average fast Dose of the discharged fuel elements (10^{21} EDN)		3.16	
Maximum fast Dose		3.68	

2.4 Comparison of Cases A and B

The question which of the two layout variants presented should be investigated in greater detail, will now be decided on the basis of the VSOP computations, although these calculations do not indicate how effective the control rods or burnable poisons will be.

2.4.1 Use of Heavy Metal in the Fuel Element

The limiting value of the volume loading for the pressed block is about 40 % for satisfactory long-term performance under irradiation.

Max. volume loading in %: 20.13 in Case A
27.43 in Case B.

Even with a high heavy-metal content (Case B), the volume loading is far below the limiting value.

2.4.2 Burn-up and Fast Dose

Here the limiting values controlling the layout are

120000 MWd/t for the maximum burn-up
5.3×10^{21} EDN for the maximum dose.

For the discharged elements, the values shown in Table 9 were determined in the cases A and B.

Table 9

	Burn-up (GWd/t)		fast Dose (10^{21} EDN)	
Case	Max.	Average	Max.	Average
A	113.5	99.2	3.59	3.14
B	83.9	68.5	3.68	3.16

2.4.3 Heavy Metal-Inventory and Depletion

If the heavy-metal content in the three recharged fuel element types are considered in fresh and burnt-up states, the difference of the values from cases A and B may be seen from Table 10.

Table 10

	Charge B-A (kg)	Discharge B-A (kg)	Depletion B-A (kg)
Th232	3664.2	3518.4	145.3
U235	-18.5	36.52	-55.0
U233	-	84.8	-

Clearly the case with high heavy-metal content can put up with somewhat less fissile material in the fresh fuel elements. Moreover, more U 233 is bred and consumed for power generation in case B during the life of the elements because of the high U 235 discharge quantity in case B. Fig. 3 tracks a fuel element-layer during its life in the core and shows the axial variation of U 235 and U 233.

2.4.4 k_{eff}, Leakage, and Necessary Excess Reactivity for X_e-Override

The lower absorption rate in thorium and the resulting lower conversion rate causes the case A k_{eff} vs. time characteristic (Fig. 4) to be higher and steeper than in case B. This means that over 40 % more burnable poison has to be used in case A.

The mean leakage in case A is over 10 % higher because of the higher neutron flux in the upper core region resulting from lower absorption. For a load variation of 100-40-100 %, case A requires an excess reactivity that is higher by 0.2 % at the beginning and 0.4 % at the end.

2.4.5 Axial Power, fast Dose and Temperature Distribution

Fig. 5, 6, 7 and 8 show the axial power, fast dose and temperature distributions in four radial regions for cases A and B. In each case, there is little difference of the axial power distribution in radial regions.

Although no gagging was applied to the gas flow, the outlet gas temperatures of the four radial regions were almost identical,

the maximum difference being 16°C in case A and 12°C in case B. The maximum surface temperatures T_o and centre temperatures T_z that were computed with due account of the temperature and dose dependence of the thermal conductivity are T_o = 963°C and 961, T_z = 1069°C and 1010°C in cases A and B, respectively.

Fig. 9 shows the axial temperature distributions of both cases and can be explained by the related power distributions. The maximum centre temperature occurs in the uppermost quarter of the core in case A and in the lowest quarter in case B.

If now a Fort St. Vrain geometry block is taken in place of the Monolith (Fig. 2), then even lower T_z and T_o should be expected. In a following chapter calculations will be quoted for monolithic fuel elements with the 8-row, 9-row, and 10-row geometry from GGA.

2.4.6 Fuel Cycle Costs of the Equilibrium Core

These costs in case B are about 6 % lower than in case A where the higher cost of fuel consumption is not offset by the lower manufacturing cost and lower breed-material consumption.

2.5 Satisfactory Core Layout

The core with a high heavy metal density has better performance characteristics than that with a low fertile content from the viewpoint of neutron physics and economy. The maximal fuel centre temperature is 1010°C in case B. which is 25 % less than the permissible value (1350°C). Should fission-product release calculations confirm this limiting value, then the outlet gas temperature could be substantially increased.

Moreover, the results presented confirm the advantages enumerated in the introduction when axial pushthrough charging is applied:

a. The radial power distribution is nearly constant in the radial three-region core considered. Since only equal-age fuel elements are positioned on the same level, there are no age-factors present as customary for HTGR with the present charge scheme. This results in reduction of the maximal fuel centre temperature and the feasibility of eliminating the costly gagging system as it has been done in the temperature calculations.

b. The satisfactory axial power distribution allows almost constant fuel temperatures above the core height because the region of highest power is in the upper cold quarter of the core.

c. The blocks are in the region of the highest fast flux for a short time only, which makes for a lower accumulated maximal dose of the fuel element. This in combination with the lower fuel temperature can provide advantages in the release of fission products.

d. The power peaks with standard charging, caused by the age differences, call for a control of the coolant-gas flow. Apart from the pressure drop caused by the control mechanisms, the "high-power regions" require a particularly intense cooling and, hence, a high gas throughput resulting in an additional pressure drop. In the axial pushthrough charging method, the gas throughput through the individual columns is also homogeneous because of the equal radial power distribution. Moreover, the gagging system can be eliminated altogether.

3. Determining the Most Satisfactory Fuel Elements

It has been shown that the core with high heavy-metal content is more satisfactory than that with a lower content both from neutron-physical and economic aspects. Now the most satisfactory geometry of the monolithic block element will be determined from the following choice:

1. the monolithic block element optimized by HRB shown in Fig. 2 (HRB block) that has been used in the above described core calculations;
2. a monolith with the geometry of the GGA block provided for a 1160-MWe HTR (8-row block, Fig. 10);
3. a monolith with the geometry of the GGA-layouted HHT block element (9-row block, Fig. 11);
4. a monolith with the geometry of the Fort St. Vrain block element (10-row block, Fig. 12).

The weighting criteria in this selection will be the maximum T_o and T_z occuring with the different block types, the pressure drop, sensitivity to power fluctuations, and the costs involved.

3.1 The Block Types

The most important data of the blocks without control rod channels are given in Table 11.

Table 11 Block Data (all dimensions in mm)

	HRB-Block	8-row Block	9-row Block	10-row Block
Fuel channels (FC)	138	132	168	210
Cooling channels (CC)	72	72	90	108
Pitch	23.00	22.99	20.70	18.80
FC-Diameter	19.00	15.85	13.97	12.70
CC-Diameter	19.00	20.98	18.44	15.88

Block height	793
Width over flats	360

3.2 Results

To compare the four block types of Table 11, the power distribution of case B was employed for computation of temperatures and pressure drop.

3.2.1 Temperatures for egual Power Distributions

Fig. 13 shows the T_z and T_o characteristics, computed on the basis of a temperature and dose-dependent thermal conductivity, for the four block types.

It will be seen that, with the given power distribution, a uniform central temperature T_z can be achieved only with the HRB and the 8-row block. For the 9-row and 10-row blocks, with their better cooling performance, a higher power in the upper core region

would be required to adjust for a homogeneous central temperature (see 3.4).
The maximum T_z and T_o values that occurred, may be seen from Table 12.

Table 12 Maximum T_z and T_o in ^oC for equal power distribution

	HRB-Block	8-row Block	9-row Block	10-row Block
T_z	1009	1011	992	975
T_o	960	963	953	941

3.2.2 Pressure drop

The pressure drop Δp listed in Table 13 refer only to the block core; loss by top and bottom reflectors and by gas ducts have not been considered.

Table 13 Pressure drop in bar within core

	HRB-Block	8-row Block	9-row Block	10-row Block
Δp	0.2537	0.1704	0.2055	0.3036

The higher pressure drop of the HRB-block as compared with the similar 8-row block results from the fact that the HRB-block stream area is about 18 % less than of the 8-row block.

3.2.3 Volume loading (FF)

The 8, 9 and 10 row-blocks have smaller fuel-channel diameters and therefore the maximum volume loading are shown in Table 14 for the desired heavy-metal inventory.

Table 14 Maximum FF in per cent

	HRB-Block	8-row Block	9-row Block	10-row Block
FF	27.43	41.21	41.68	40.34

These FF are all in a range realistic with a monolith. With the particle concept chosen, the FF limit can be assumed as about 40 %.

3.2.4 Temperatures for Most Satisfactory Power Distribution

It can be seen from Fig. 13 that a new power distribution has to be found for the 9 and 10 row-blocks in order to adjust a constant T_z. Fig. 14 shows the power distributions most favorable for the individual block types. The maximum surface temperatures T_o and centre temperatures T_z have been compiled in Table 15.

Table 15 T_z and T_o in °C for most favorable power distribution

	HRB-Block	8-row Block	9-row Block	10-row Block
T_z	1009	1011	979	954
T_o	960	963	943	924

All four block types have T_z well below the limit of 1350°C so that satisfactory fission-product release values can be expected from the 10-row block in particular.

3.2.5 Power Fluctuation

This section is concerned with the investigation how the core will respond in its temperature attitude when the power distribution adjusted is changed. Generally it may be said that the core is rather insensitive to power variations. Table 16 shows the per-cent increase of T_z with a variation of the maximum relative power by about 13 % for the four block types considered.

Table 16 Change of T_z when max. relative power is increased by 12.7%

HRB-Block	8-row Block	9-row Block	10-row Block
+ 6.1 %	+ 6.1 %	+ 6.0 %	+ 5.3 %

3.3 Most Satisfactory Fuel Element

Based on the results achieved, the 10 row-block was selected for further and more detailed investigation although a higher pressure drop in the core and higher fuel cycle costs had to be put up with.

In a core of 10-row blocks, the pressure drop is almost 80 % higher than in a core with 8-row blocks. Since, however, the absolute pressure drop is minor, no effect upon system efficiency is to be expected.
The total fuel cycle cost taking the 10-row block is only about 1.3 % higher than the FCC with the HRB-block although the fabrication cost is for the 10-row block about 25 % dearer.

Contrariwise, the advantages of the 10-row blocks refer to the cooling where the T_z and T_o are 60°C and 40°C, respectively, less than for the 8-row block for an outlet gas temperature or turbine inlet gas temperature of 850°C. This fact indicates that more satisfactory fission-product release rates can be expected from the 10-row block regardless of the outlet gas temperature chosen. Moreover, the 10-row block offers the possibility of achieving higher gas outlet temperatures and a greater insensitivity towards power fluctuations.

4. Conclusion

With the axial push-through fuel management one achieves satisfactory neutron-physical and thermodynamic conditions. Furthermore a high potential with respect to higher gas outlet temperatures can be assumed, only limited by the allowable fission product release. The great flexibility of the core with high heavy-metal inventory and the satisfactory cooling properties of the 10-row bloc permit adjustment of almost any power distribution desired in order to achieve low fission-product release rates. If all engineering problems of the charge and discharge operations can be solved, the axial push-through could be a desirable fuel management scheme.

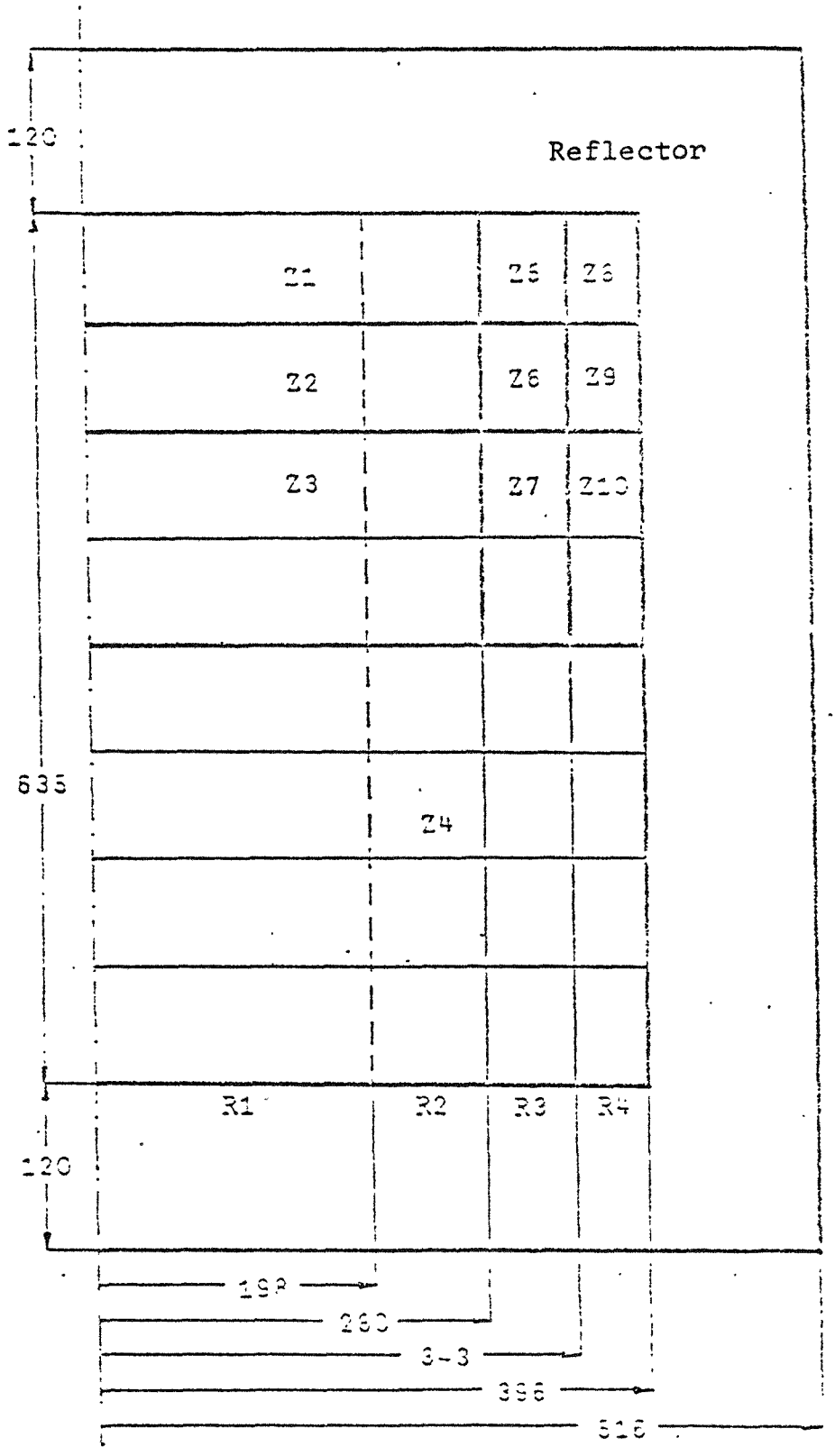

Fig. 1: Coremodel as used in VOSP
(Dimensions in cm)

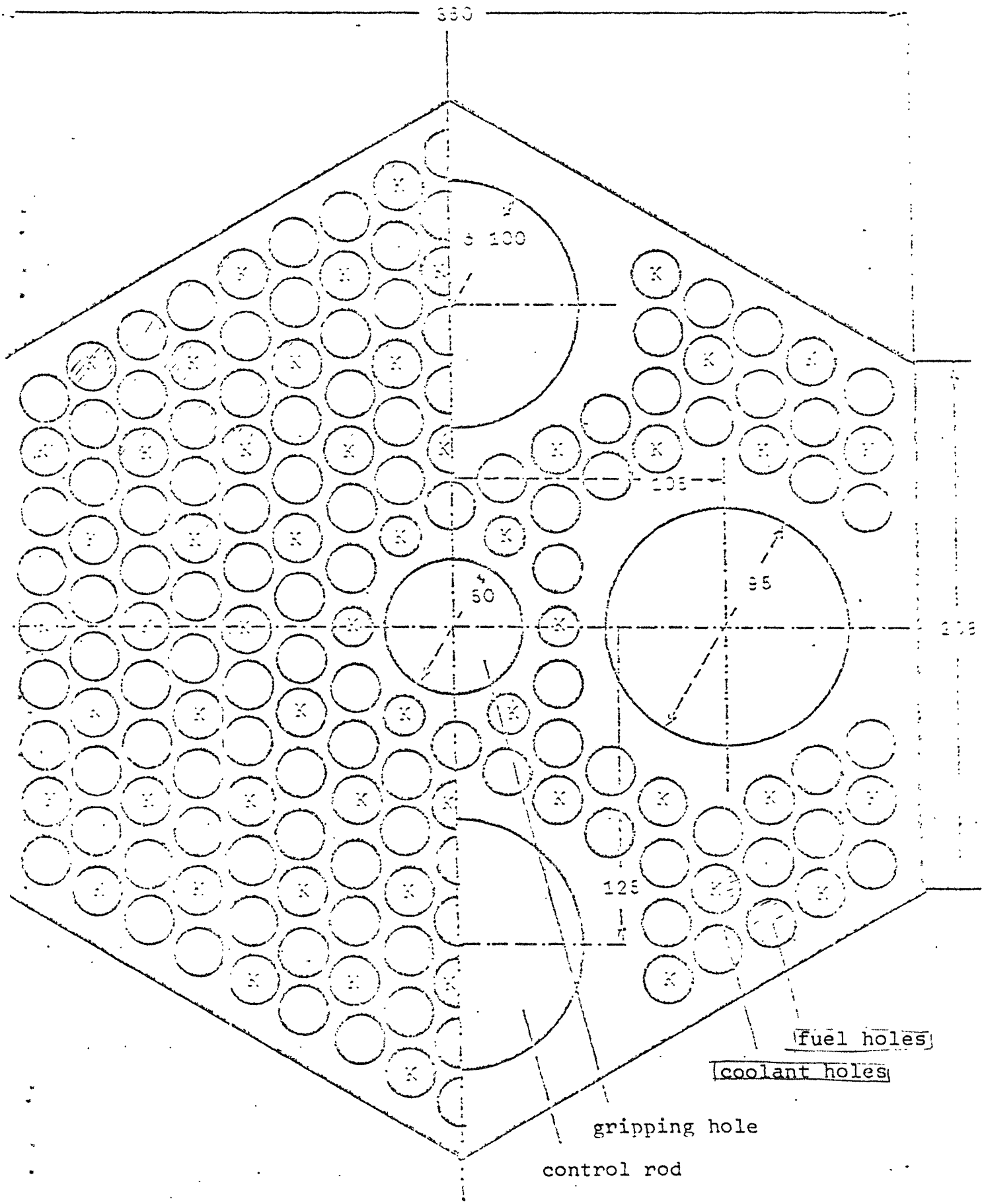

Fig. 2: Monolith-Fuelelement

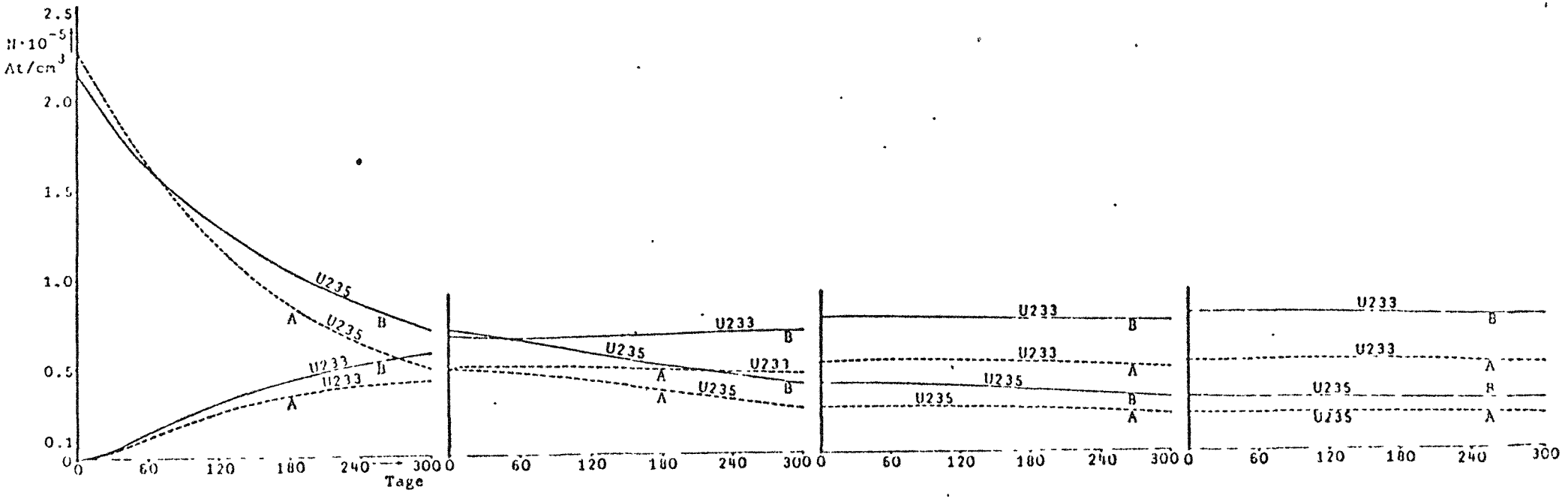

Fig. 3: Variation with time of fissile inventory

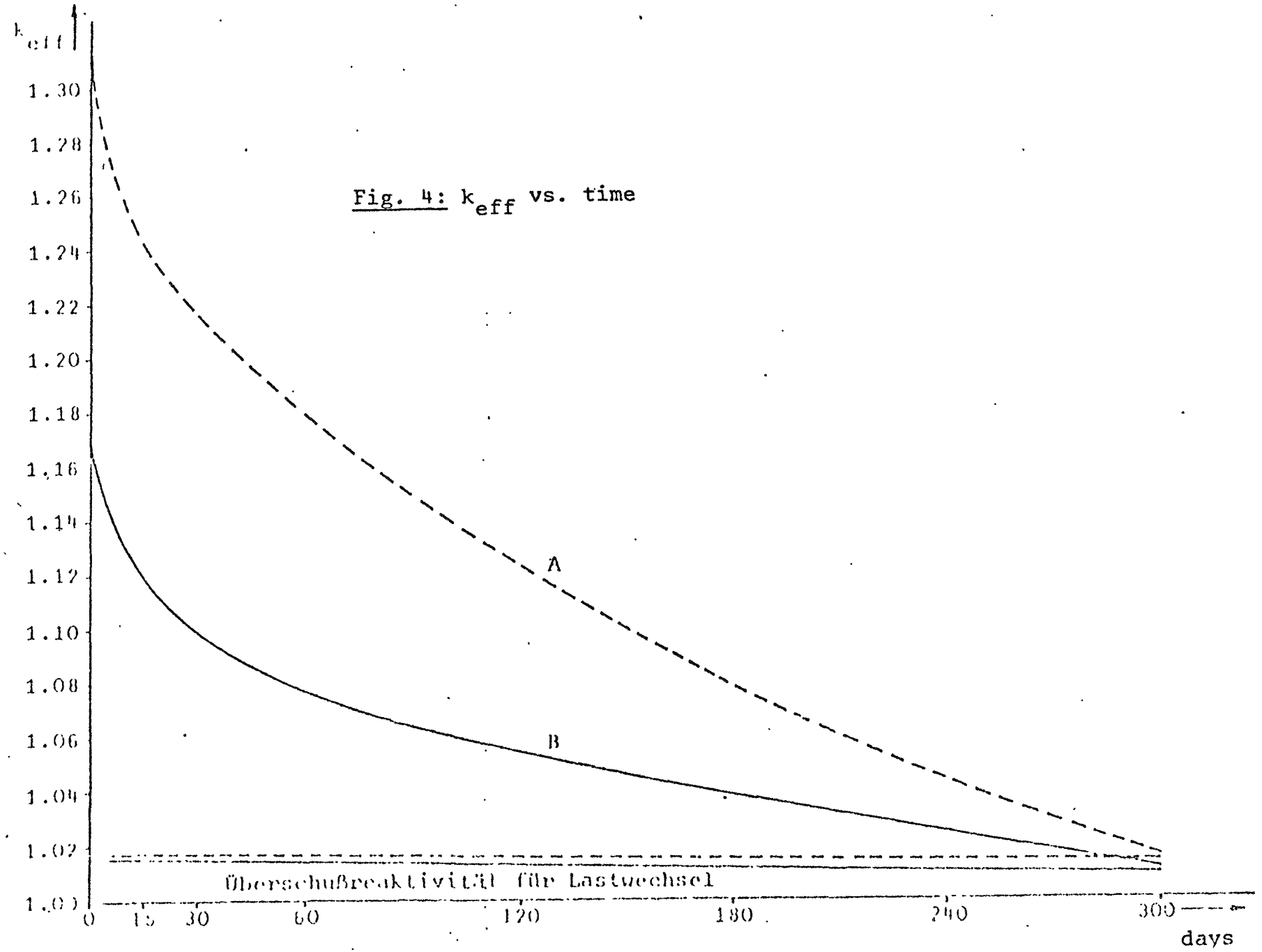

Fig. 4: k_{eff} vs. time

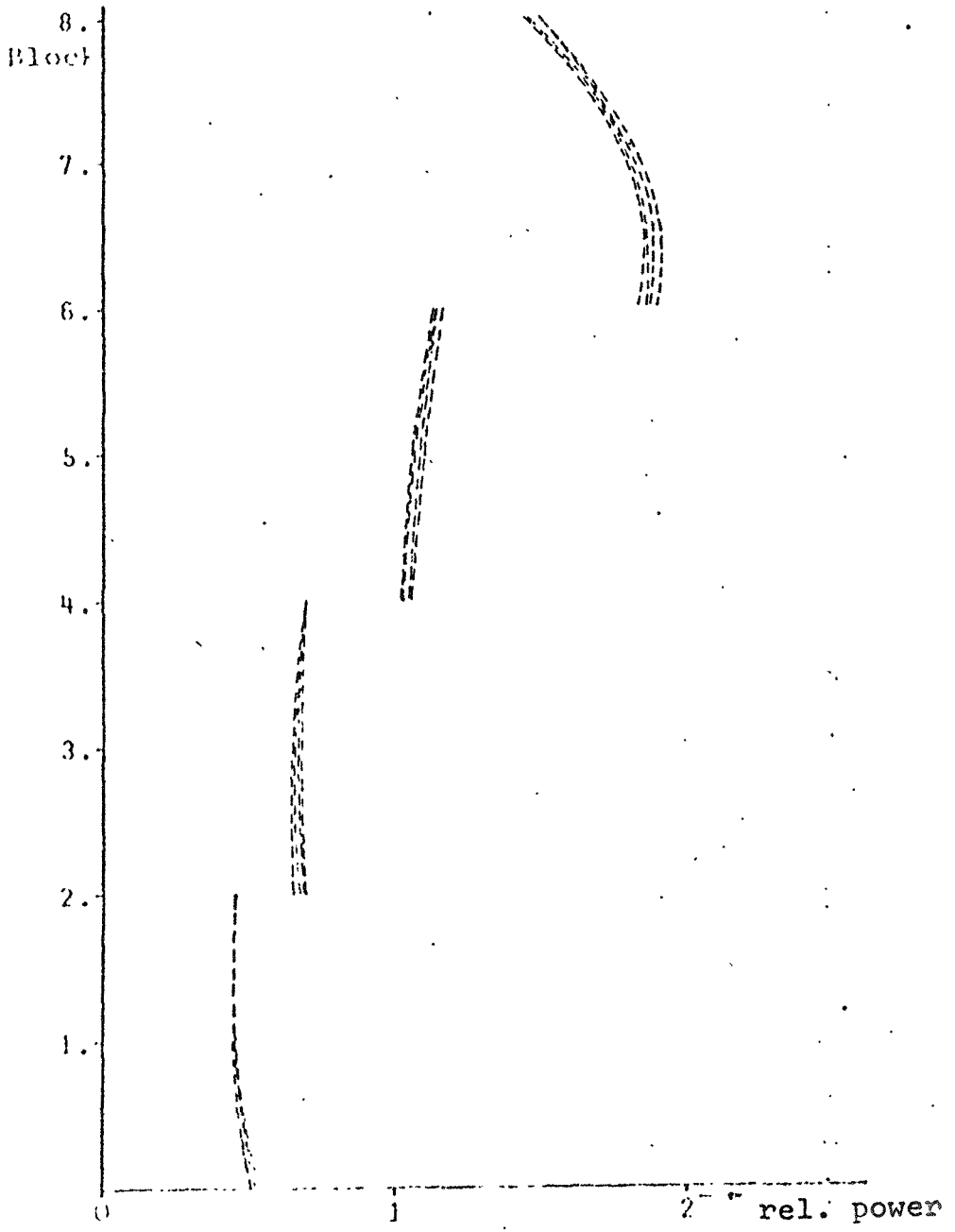

Fig. 5a: Axial powershape in the four radial zones (Case A)

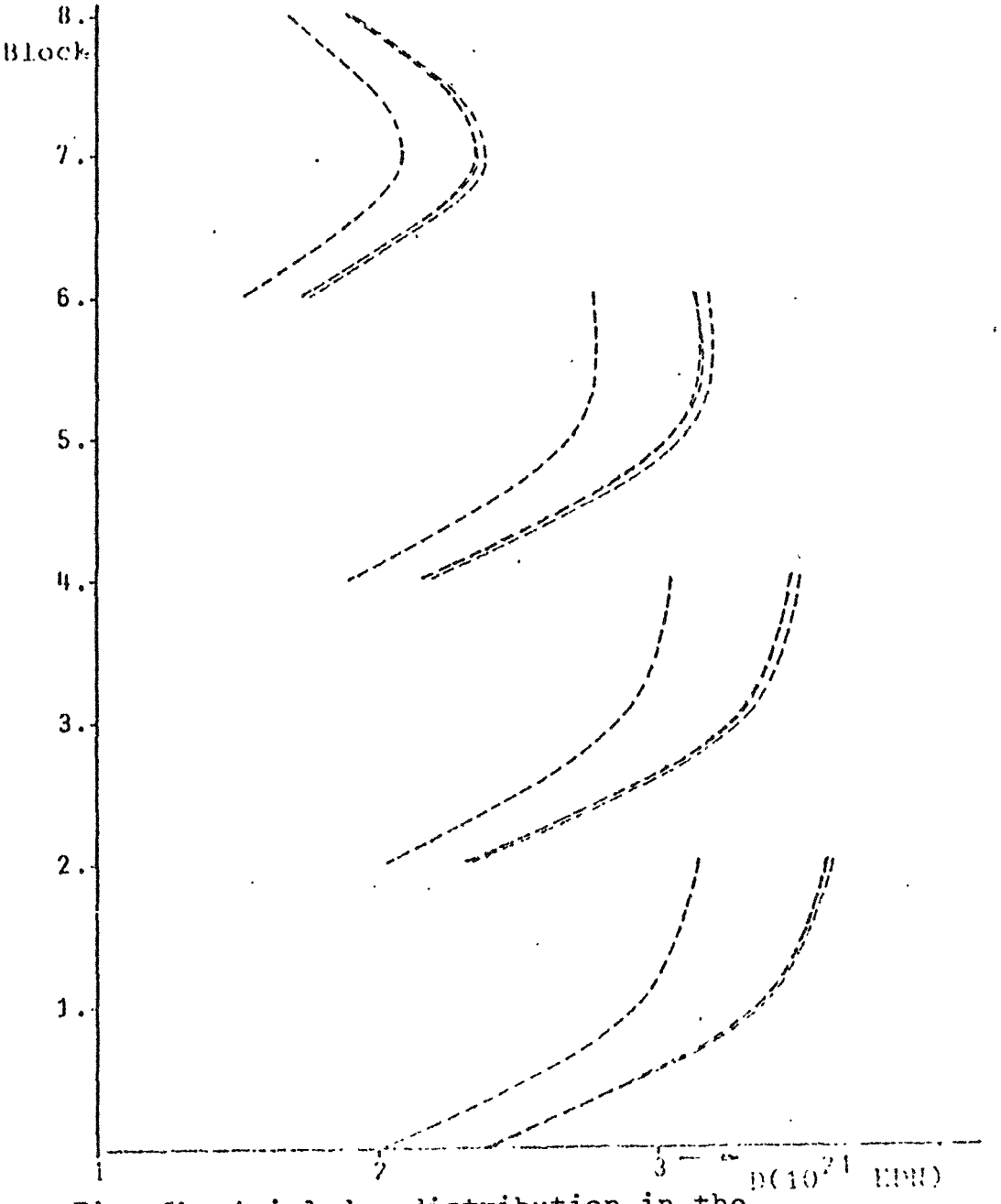

Fig. 5b: Axial dosedistribution in the four radial zones (Case A)

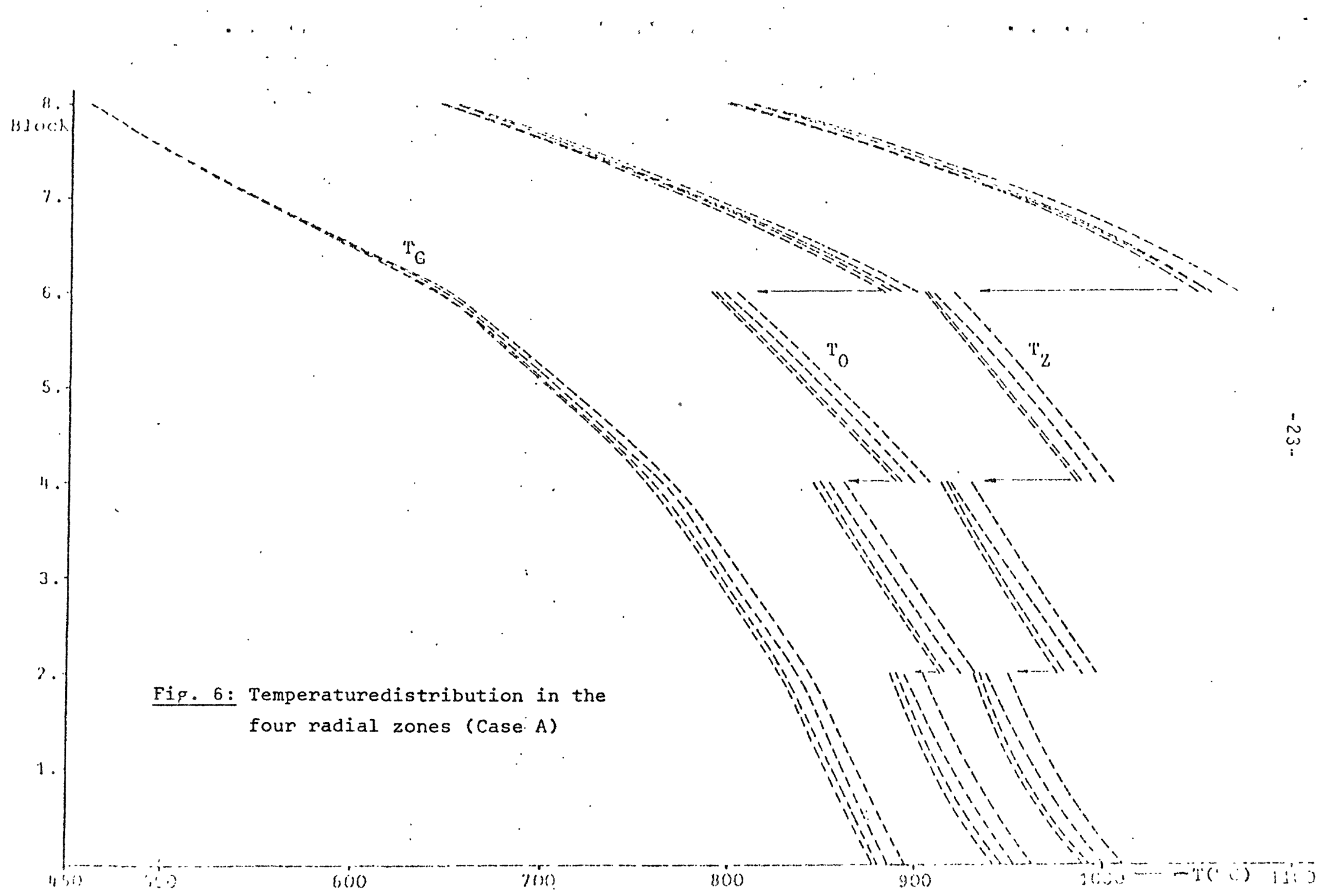

Fig. 6: Temperaturedistribution in the four radial zones (Case A)

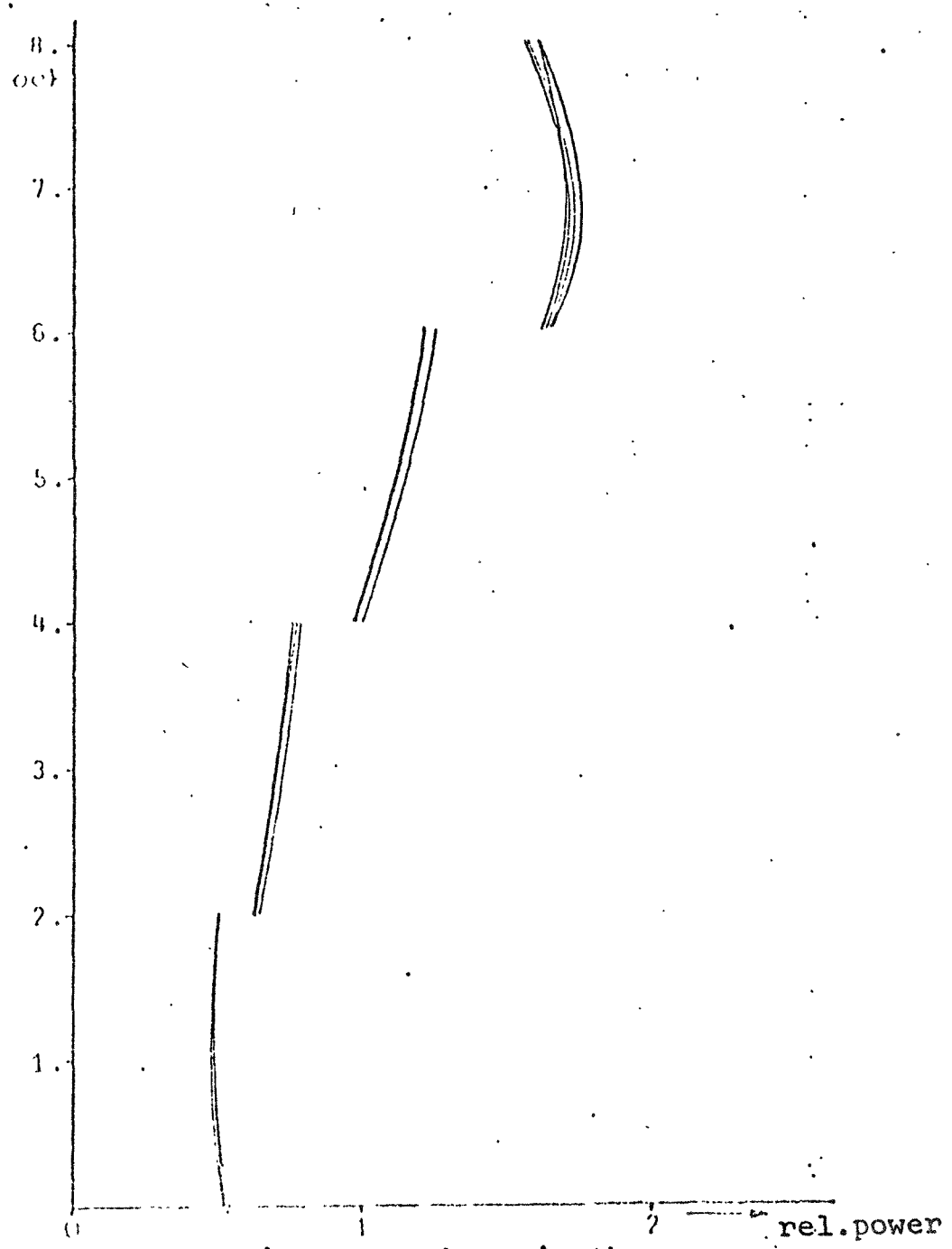

Fig. 7a: Axial powershape in the four radial zones (Case B)

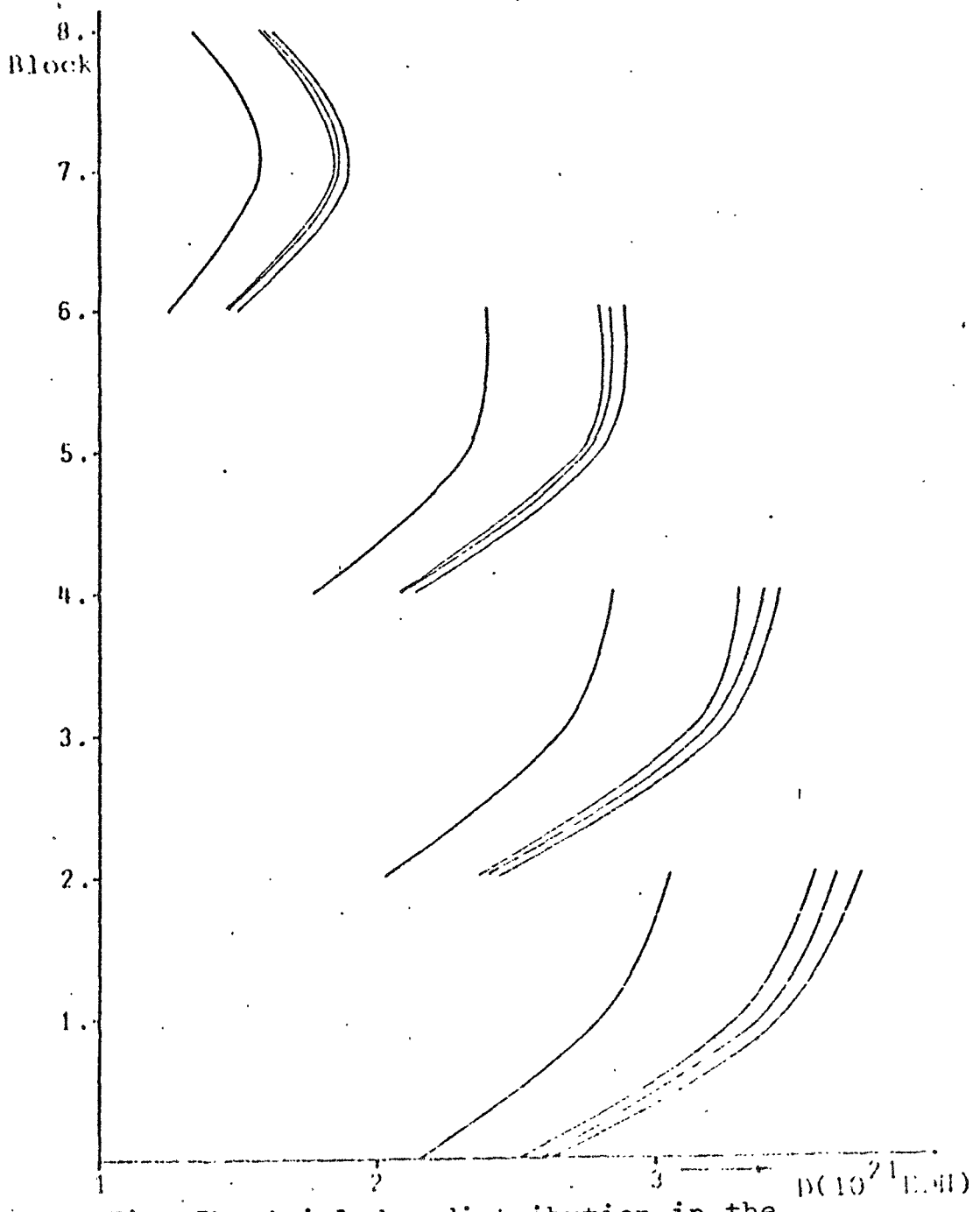

Fig. 7b: Axial dosedistribution in the four radial zones (Case B)

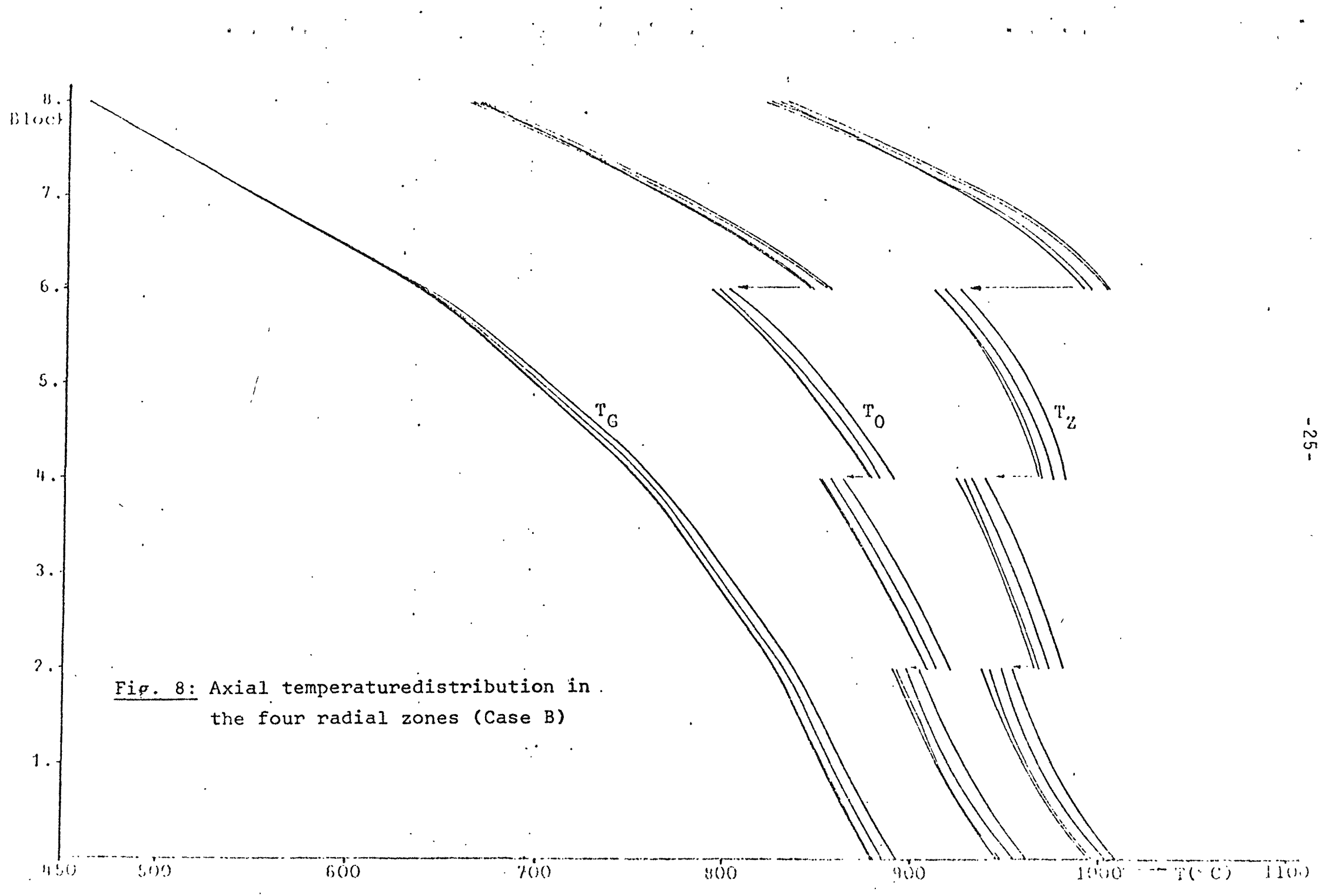

Fig. 8: Axial temperaturedistribution in the four radial zones (Case B)

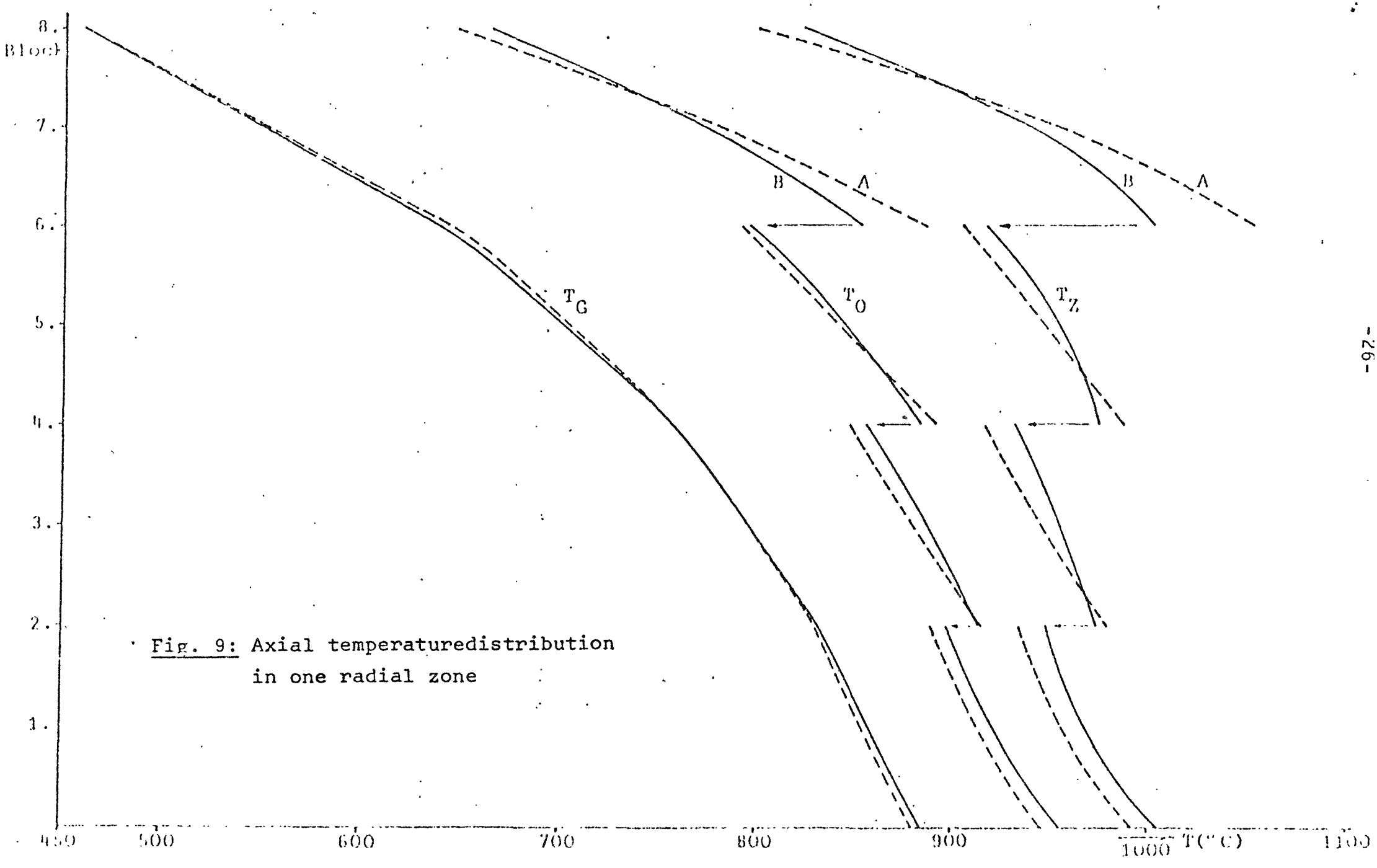

Fig. 9: Axial temperaturedistribution in one radial zone

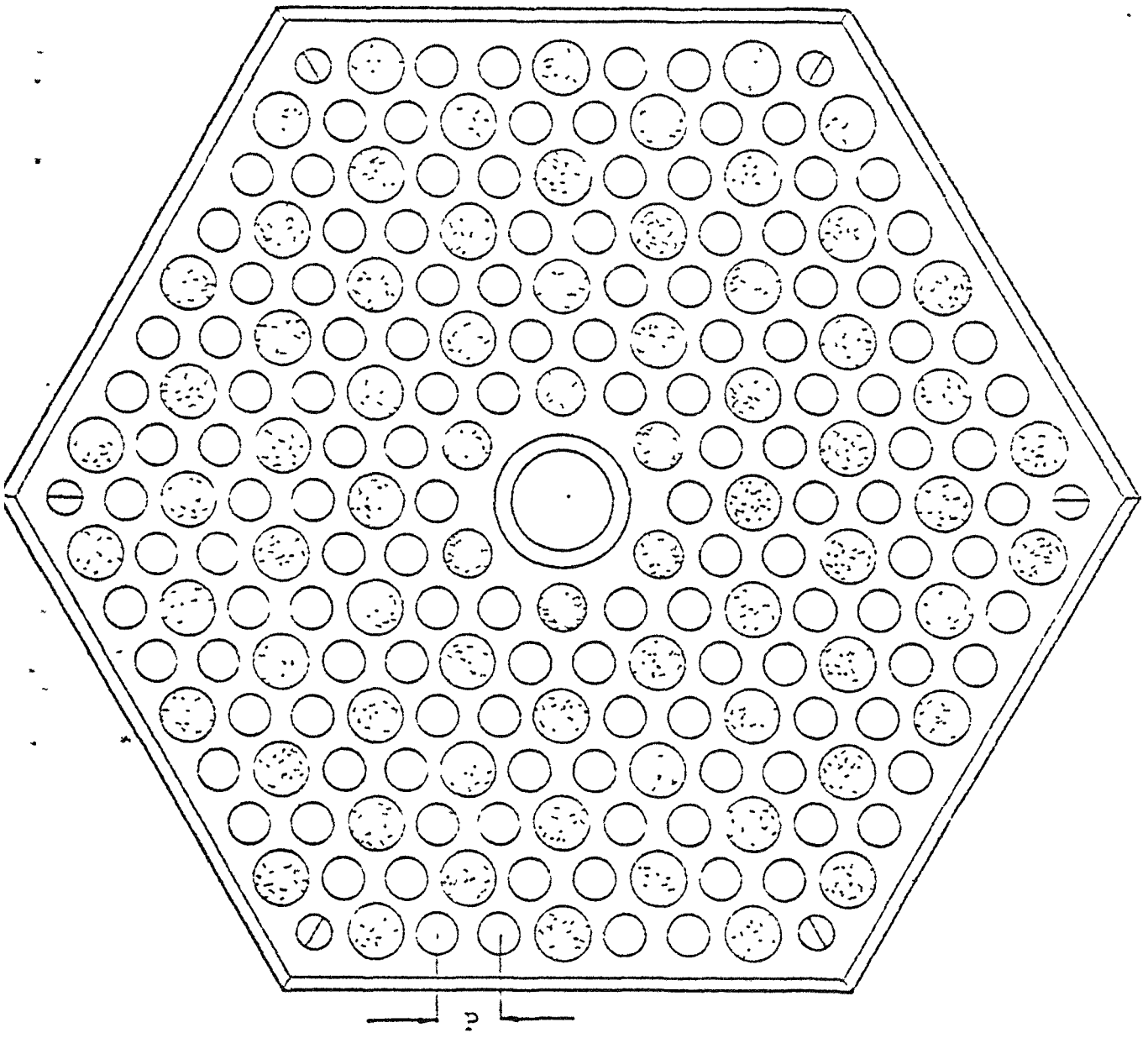

P=pitch=22.99 mm

poison holes

fuel holes 15.85 mm$^{\emptyset}$

coolant holes 18.26 mm$^{\emptyset}$

coolant holes 20.98 mm$^{\emptyset}$

Fig. 10: GGA-fuelelement for a 1160 MW_e-reactor ("8-row Block", 132 fuel holes)

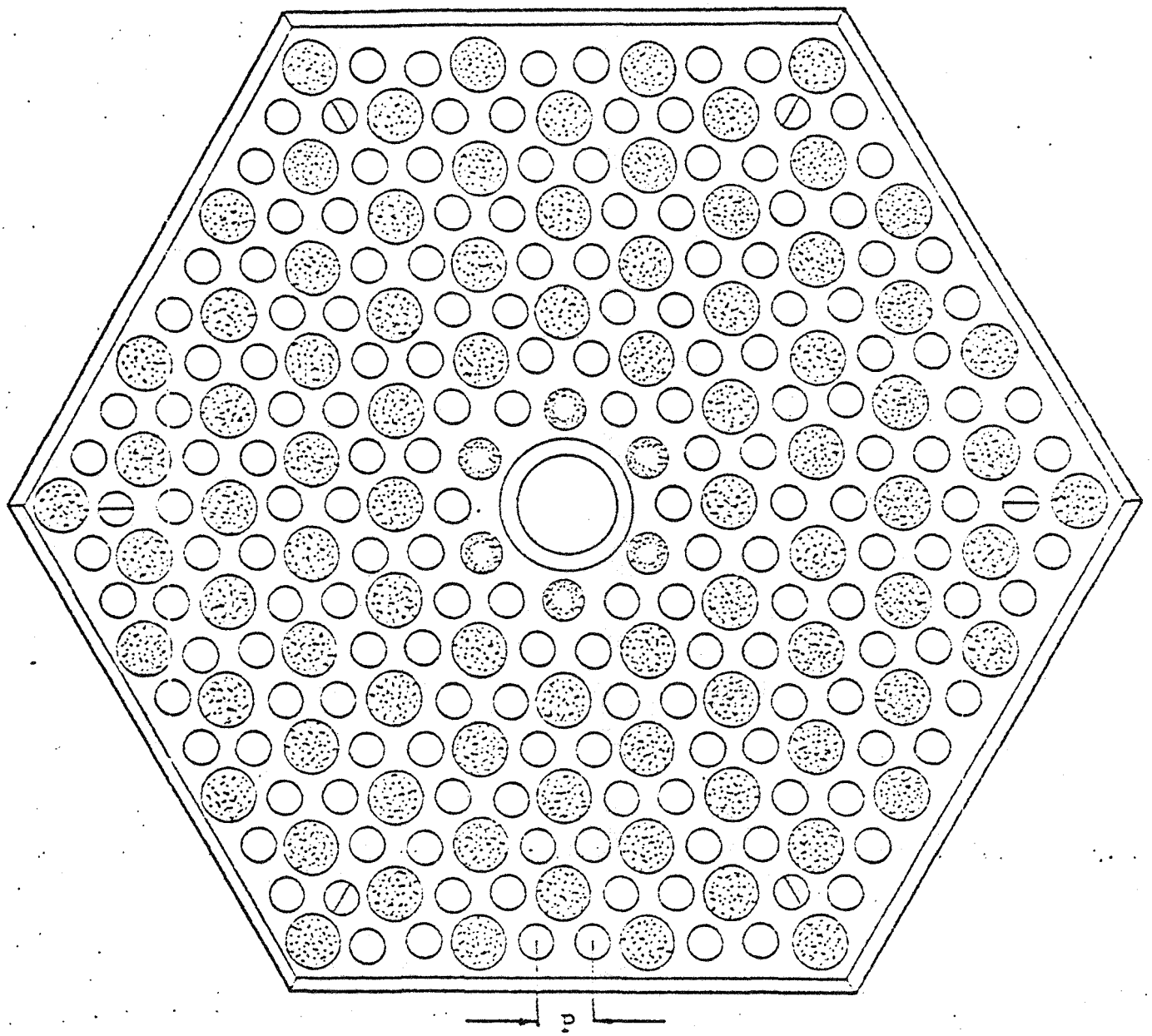

P=pitch=20.70 mm

⊖ poison holes

○ fuel holes 13.97 mm$^{\varnothing}$

coolant holes 15.75 mm$^{\varnothing}$

coolant holes 18.44 mm$^{\varnothing}$

Fig. 11: GGA-fuelelement for a 1000 MW_e-HHT ("9-row Block", 168 fuel holes)

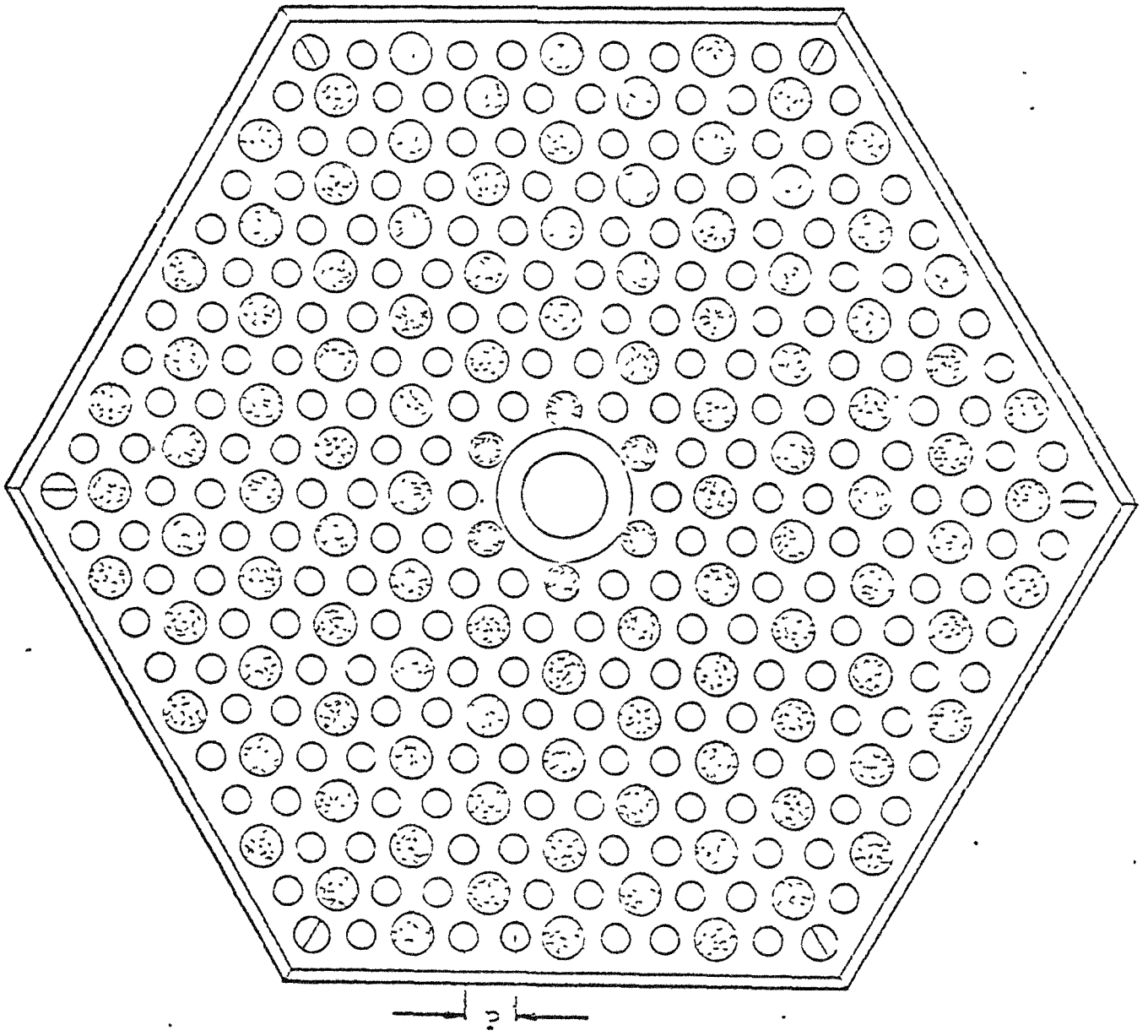

P=pitch=18.80 mm

poison holes

fuel holes 12.70 mm$^{\emptyset}$

coolant holes 13.46 mm$^{\emptyset}$

coolant holes 15.88 mm$^{\emptyset}$

Fig. 12: GGA-fuelelement for the Fort St. Vrain reactor("10-row Block",210 fuel holes)

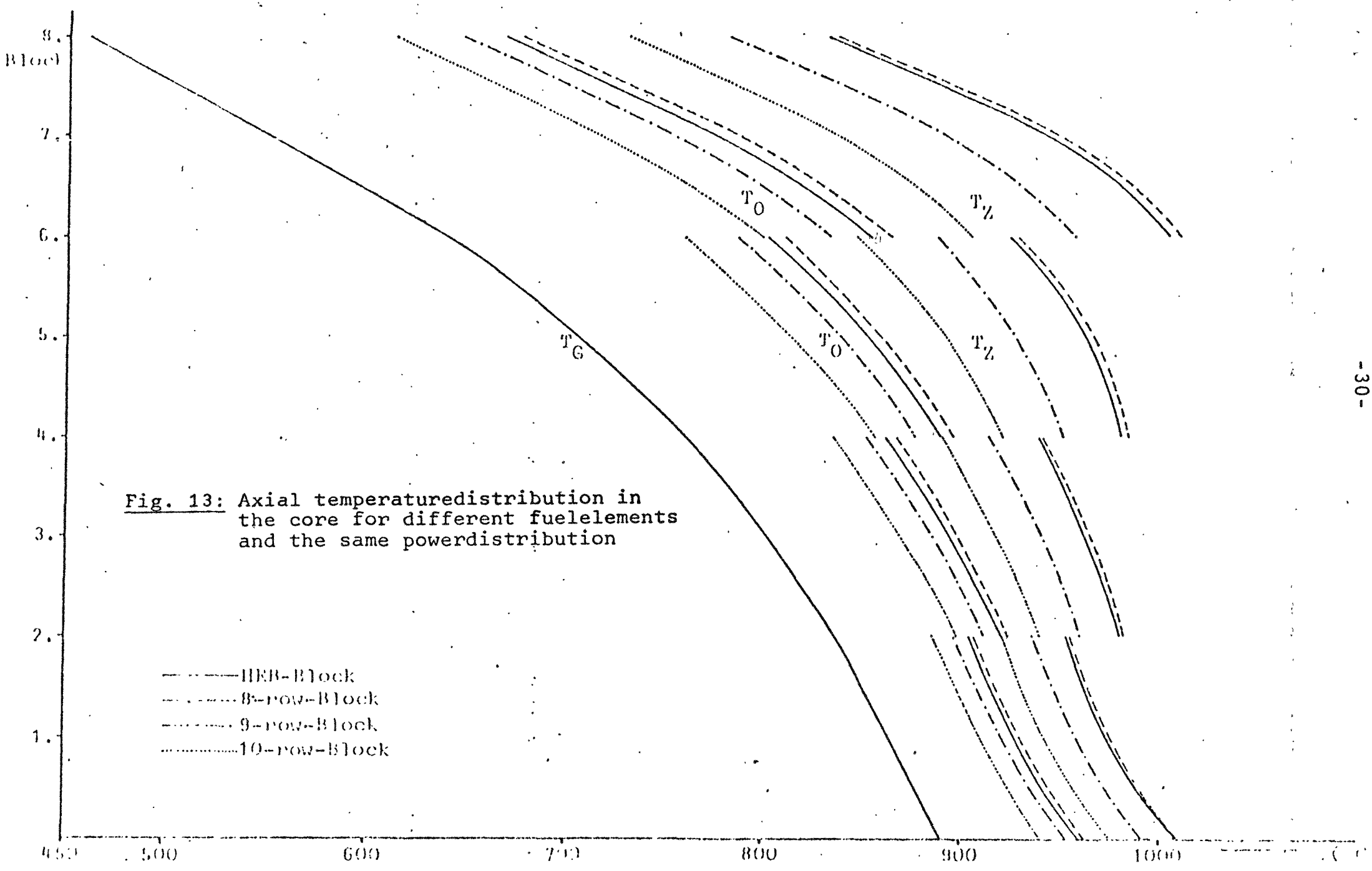

Fig. 13: Axial temperaturedistribution in the core for different fuelelements and the same powerdistribution

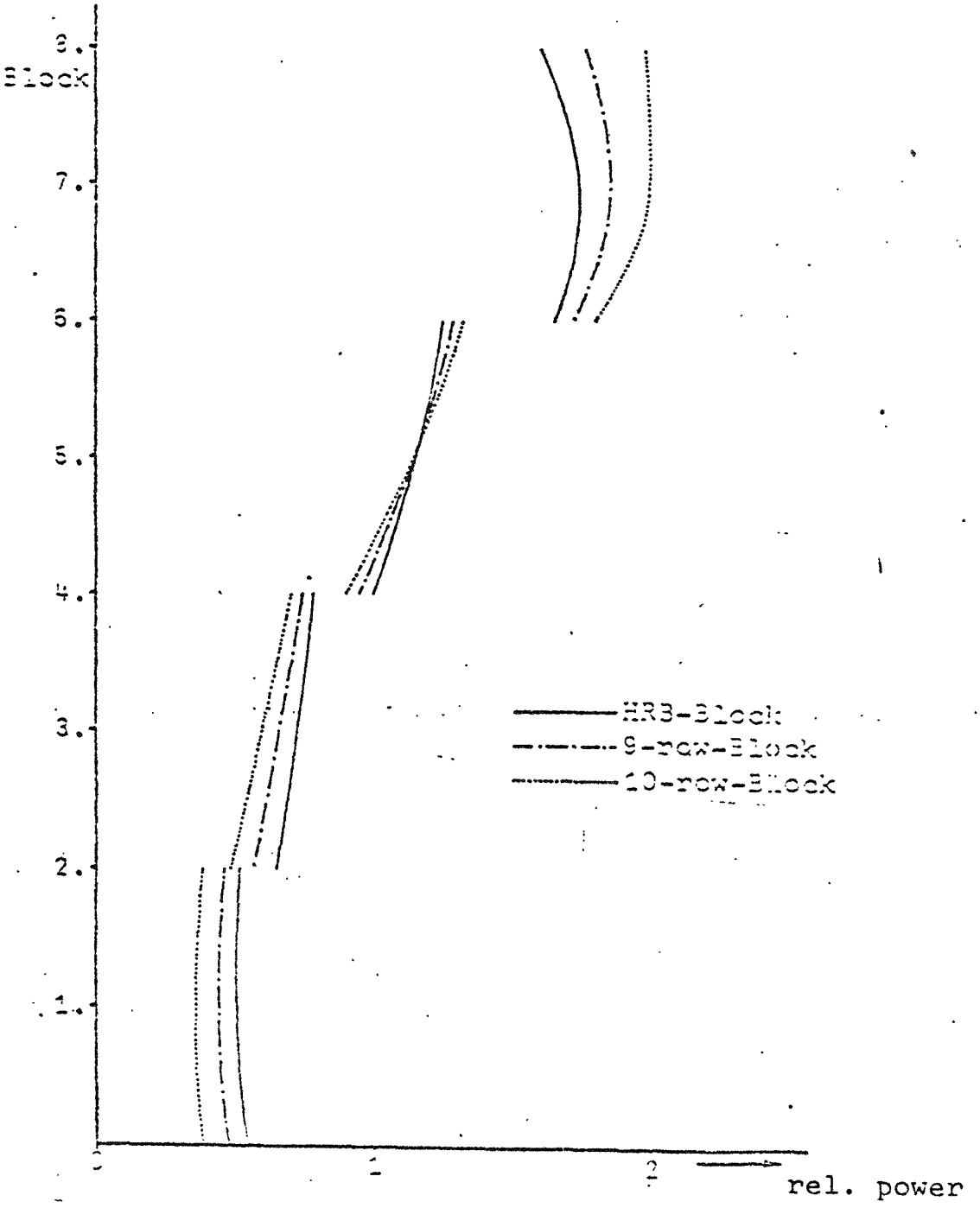

Fig. 14: Satisfactory axial powershape for the different fuelelements

First Results of the "Layer Loading System" Part 2

by

Dr. A. Dworak

1. Introduction

As one can see from the results of the "Axial Push-Through" study (Part 1, Fig. 3) most fissile material is used in the two top most fuel blocks. In the bottom region of the core an equilibrium condition exists between the burn up of U-235 and the build up of U-233.
It was investigated if a system could work where only the upper part of the core is replaced after certain intervalls (e.g. after 300 full power days) to compensate there the loss of fissile material.

In this paper the first positive results of such a "Layer Loading System" (LLS) are quoted.
Some main advantages of the LLS are:

1. achieving an optimal axial and radial power distribution, this leads to a low fuel and surface temperature
2. simpler refuelling operations
3. no Age-factors - as all fuel elements in a certain layer have the same time of insertion
4. due to missing Age-factors no gagging system is needed
5. the redundant gagging system results in a lower core pressure drop and therefore an increase in the net plant-efficiency is given
6. reduction of the accumulated fast dose in the fuel elements
7. due to low temperature and fast Dose-values reduced fission product release can be assumed
8. no running in cycle is needed
9. at the end of a LLS-period a total core-inspection is possible
10. at the end of a "LLS-period" one can switch to a different "LLS" reload plan e.g. if in the mean time the coated particle or graphite performance data have been improved.

2. Methods and Results

The methods used for this survey are the same as quoted in Part 1. The coated particle dimensions, fuel element dimensions and the main core parameters are given in Table 1, 2, 3, 4 and 11 of Part 1.
The in VSOP used core model is shown in fig. 15. For the first approach a radial one-zone- and axial 8-layer core was considered were the fuel element had the same dimensions and geometrical layout as the Fort St. Vrain 10 row-block. For further calculations a radial 3-zone core will be used which should have the same radial power distribution performance as shown in the "Axial Push-Through" study.

For the first calculations the following approach was taken:

1. to have in a rather short time some idea how to influence the axial power distribution, the axial power swing during a "LLS-Subperiod" (300 days) should be reasonable small. This led to a low N_C/N_{Th}-ratio and therefore to a low burn up (average 37 GWd/t) and to a high conversion-ratio. This means however that the core is not jet cost-optimized

2. as no burnable poison could be taken into account the power distribution in question (see fig. 17 and 18) should be reached halfway through a LLS-Subperiod, e.g. after 150 days.

In fig. 16 the investigated LLS-reload plan for a 8-Subcycle-Period is shown. In this fig. the loaded material data are given as well.
In the first subcycle the core consists only of fresh fuel elements, in the second subcycle the two top most layers are replaced. In the third and fourth subcycle three layers will be replaced, and so on .....
At the end of the 8^{th}-subcycle the whole core will be replaced and a new LLS-Period will start - which of course can follow a different reload scheme.
Fig. 17 shows a typical axial power and temperature distribution for the Fort St. Vrain fuel element. As an exemple the fast dose distribution at the end of the 8^{th} subcycle was taken whereas the drawn power distribution was reached at the 185^{th} day of subcycle 8.
During all 8 subcycles the mixed gasexit temperature is $850^{o}C$, the maximal fuel centre temperature is always below $950^{o}C$ and the maximal surface temperature is about $920^{o}C$.

In fig. 18 a typical power swing during a subcycle is drawn. The dotted graph shows the power distribution which should stay more or less constant over a subcycle.
The power distribution in question can be achieved and keept constant by using burnable poison in connection with the freshly loaded fuel elements(private communication WA Simon GGA). The calculation showed that without using burnable poison the propper axial power distribution is reached half way through a subcycle between the 135^{th} and 185^{th} day. A few calculation were performed to investigate how effective one can influence the axial power distribution by using poison. The results are shown in fig. 19.
In 2-D diffusion calculations the absorption cross section of graphite was in certain regions increased by a certain ammount to simulate there presence of poison at a particular time point.

Graph 1: shows the undisturbed power distribution

2: shows the axial power distribution when the σ_a (0.0253 eV) of the Top Reflector was increased by 80 mb ($\triangle$ k = -1.25 %)

3: shows the power distribution when the graphite absorption cross section of the two top moost layers is increased by 80 mb ($\triangle$k = -3.68%)

4: same as graph 3, in addition the Bottom Reflector is poisoned as well (80 mb) ($\triangle$ k = -3.78 %)

5: the graphite absorption in the two top moost layers is increased by 40 mb and the Bottom Reflector is poisoned (80 mb) ($\triangle$ k = 2.42 %)

From the results of fig. 19 it is obvious that the detailed modelling of the axial power distribution seems not too difficult. A more detailed survey to cover this aspect is in the pipeline.

Table 17

Main Core-Performance Data

	1		2		3		4		5		6		7		8	
Subperiod	Start	End	Start	End	Start	End	Start	End	Start	End	Start	End	Start	End	Start	End
Inventory [kg]																
Th 232	48122	47419	47333	46644	46778	46332	45972	45314	45904	45234	44594	43956	44061	43432	43923	43295
U 235	2214.5	1366.9	1788.5	1072.3	1695.0	1163.8	1585.1	876.5	1691.0	943.8	1412.6	748.0	1460.1	747.0	1401.6	698.6
U 233	0	435.3	302.9	621.7	363.8	584.0	449.33	730.1	362.1	682.6	538.2	764.6	505.0	760.3	539.8	784.4
k_{eff}	1.095	1.019	1.114	1.012	1.119	1.013	1.138	1.012	1.129	1.012	1.159	1.004	1.165	1.011	1.165	1.007
Absorption in Fission products %	2.1	5.6	2.61	6.86	2.40	7.28	2.44	7.95	2.22	7.44	2.73	8.80	2.42	8.64	2.47	8.94
max. fast Dose 10^{21} EDN		1.80		2.19		2.16		2.85		2.20		2.60		2.86		2.91
average Burn up of Discharge Fuel elements [GWd/t]		31.0		34.0		30.0		36.0		38.5		44.0		39.0		39.0

Total amount of fissile material kg loaded in 8 years

	Charged	Discharged	△
U 235	9423.38	3608.0	5815.38
U 233	0	3023.7	-3023.7

Average Burn up GWd/t = 37.0 X_e-Override (100-40-100%) : Δk_{eff} = 1.1 %

Average Conversion ratio: 0.580

Average total leakage [%] = 3.3

Loss of Fissile Material in 8 years [%, $\eta \cong 1.15$] =

$$= \frac{\text{U 235 (Ch)} - \text{U 235 (Dch)} - \text{U 233 (Dch)} * \eta}{\text{U 235 (Ch)}} * 100 = 24.8\ \%$$

In fig. 20 the accumulated fast dose-history for all 8 subcycle in all 8 layers is drawn whereas in fig. 21 the Fraction of Fission from U 233 is given.

Conclusions

This first survey on the Layer Loading System shows that a fuel management where only horizontal layers of fuel elements in the upper core region are replaced works satisfactory and has many advantages with respect to low fuel- and surface-temperature or with respect to the potential of an increased gas outlet temperature. Further more one can assume that the low fuel- and surface temperature leads in connection with the low value of the accumulated fast dose to a reduced fission product release. Due to missing age-factors no gagging system is neccessary. An additional advantage of the LLS is that no running in cycle is needed.

Future work on this system will be done to investigate the following three aspects

1. a LLS with a higher burn up
2. other LLS
3. establish a controlrod and burnable poison management.

Table 18 Comparison between "Batch Loading System", "Axial Push-Through" and "Layer Loading System"

	BLS	APT	LLS
Surface- and Fuel Centre Temperature		++	++
Possible increase of gasoutlet temperature		++	++
achieved burn up	+	++	
max. fast Dose		+	++
Neutron economy			+
Age-Factors		+	+
Controlrod efficiency		+	+
Running in cycle		++	++
Flexibility of fuel management		+	++
reload operations	+		++
importance of possible reload error		(+) +	++
Fission product release		+	++
expected FCC	++	+	

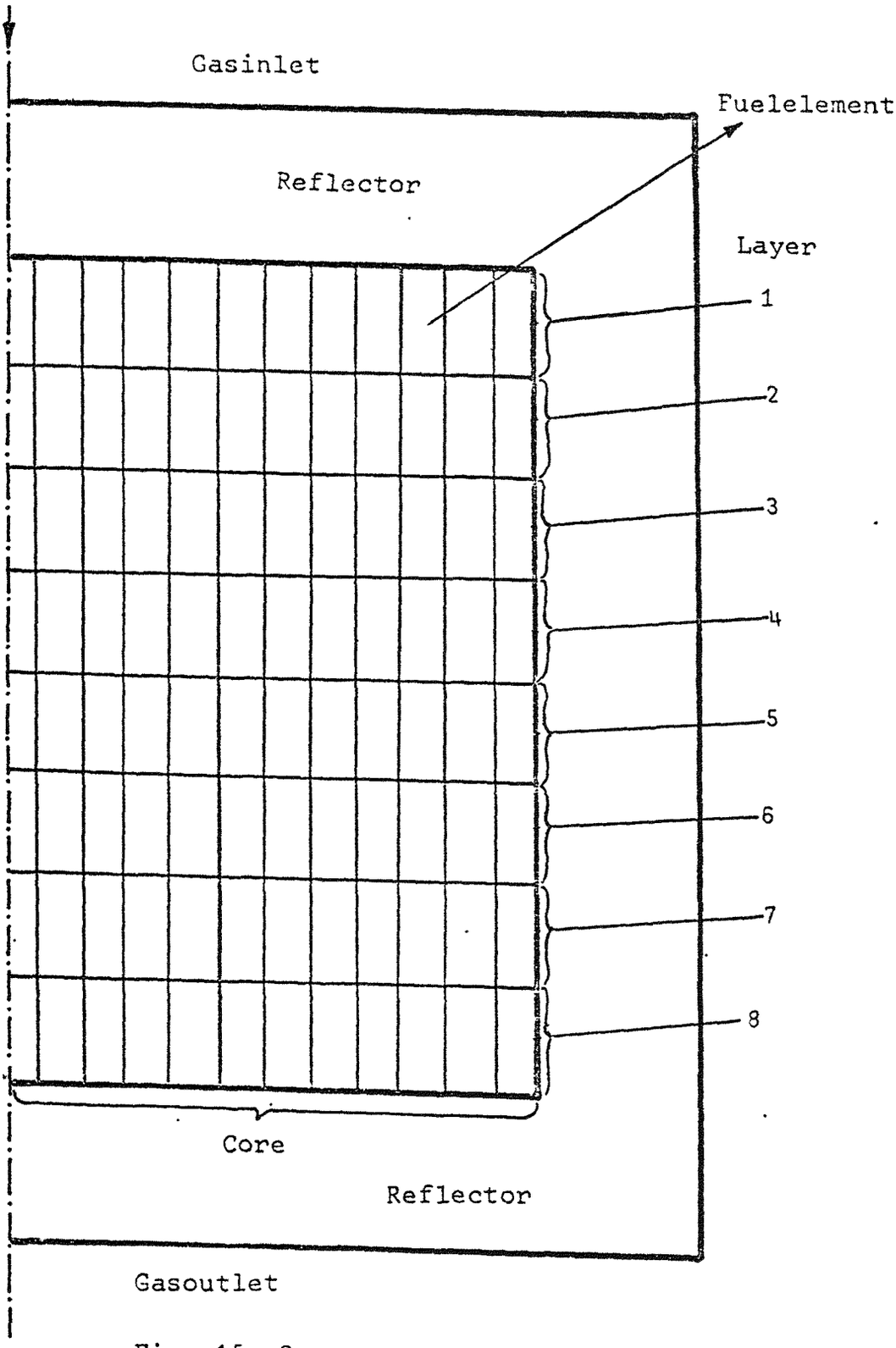

Fig. 15 Coremodel as used in VSOP

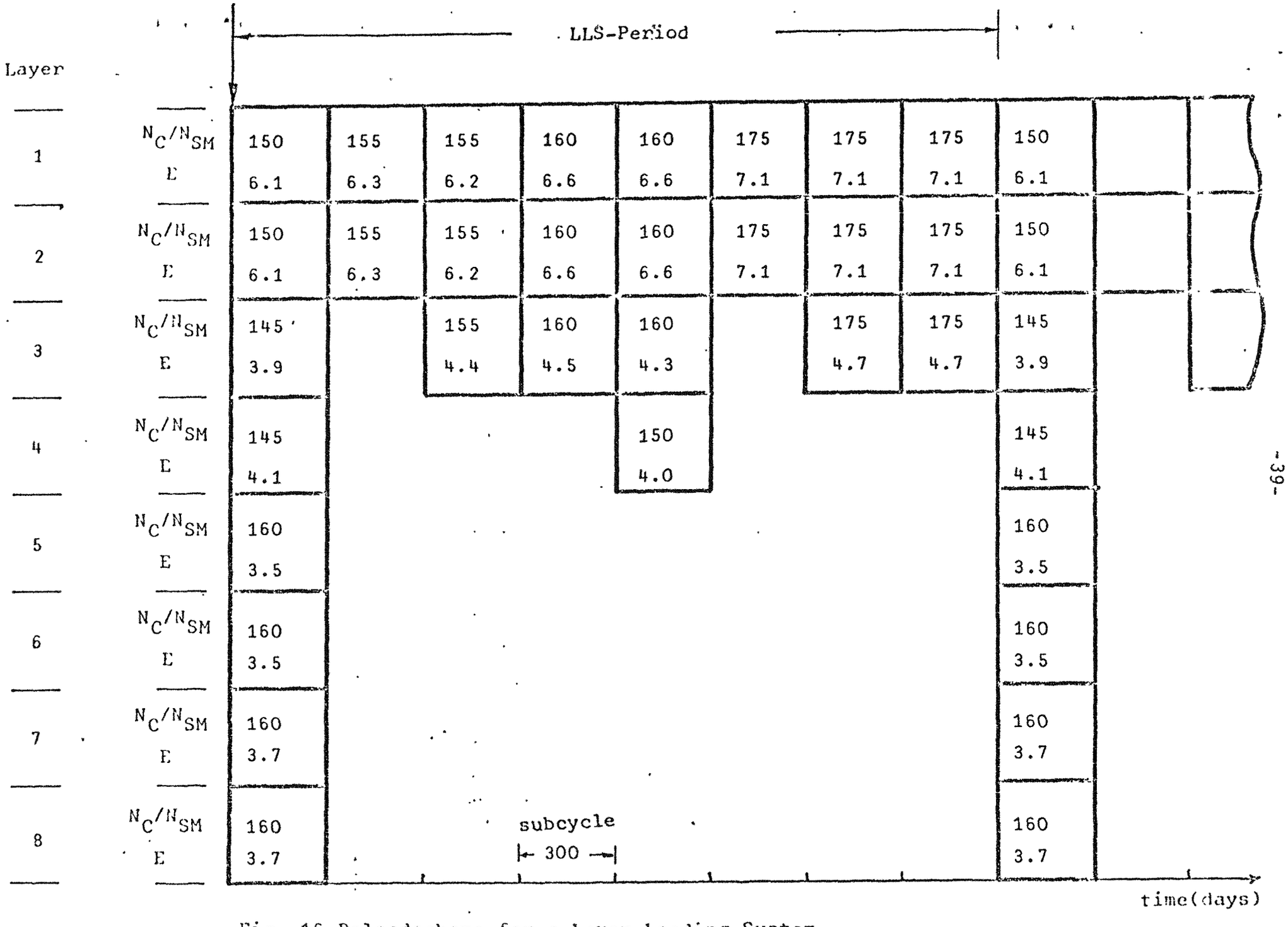

Fig. 16 Reloadscheme for a Layer Loading System

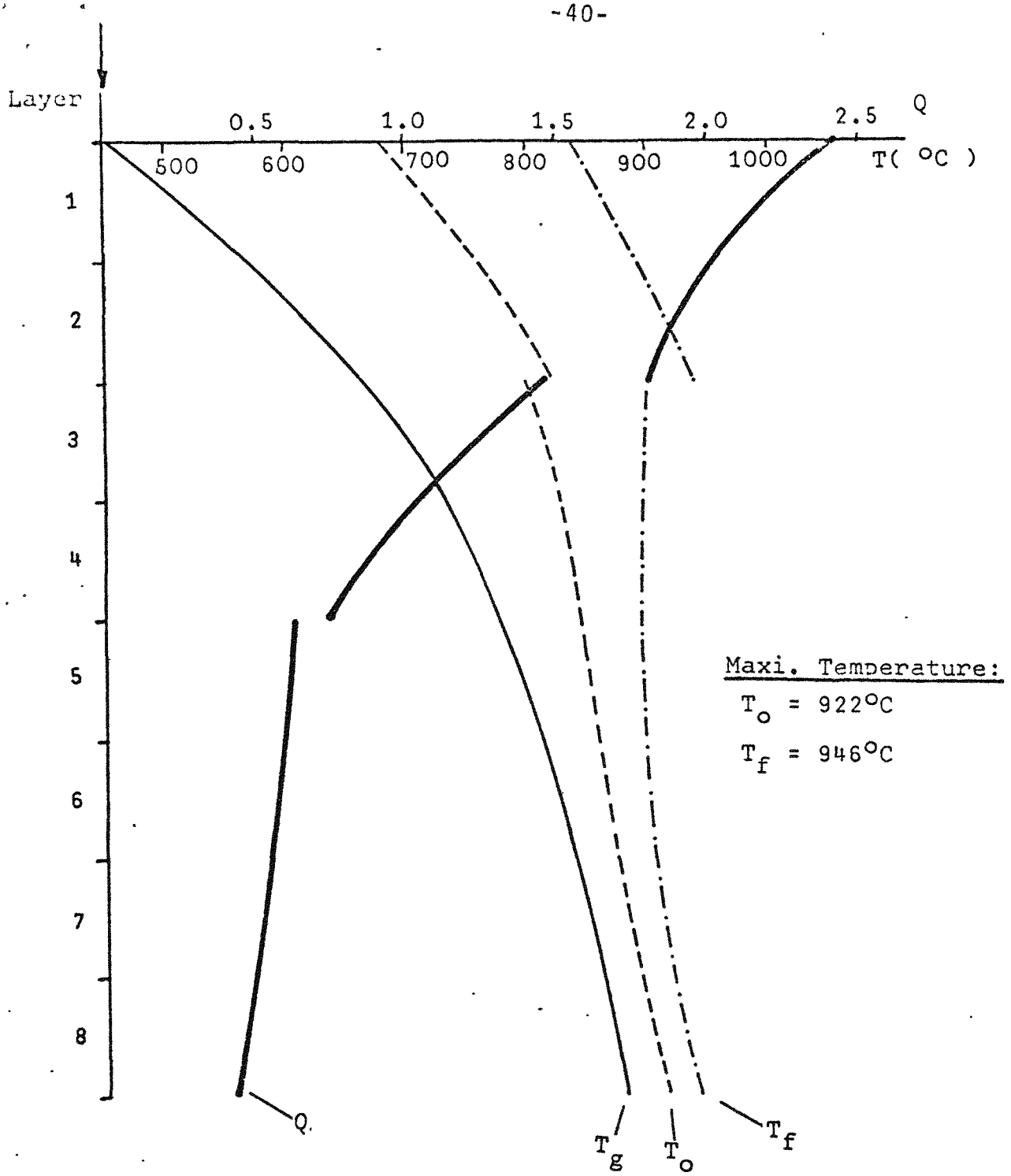

Q= Power normalised to average Corepower

T_g=Gastemperature (850°C +8% bypass =884°C

T_o=Surfacetemperature

T_f=Fuel centre temperature

Fig. 17 Axial Power and Temperature distribution (8 th Subcycle)

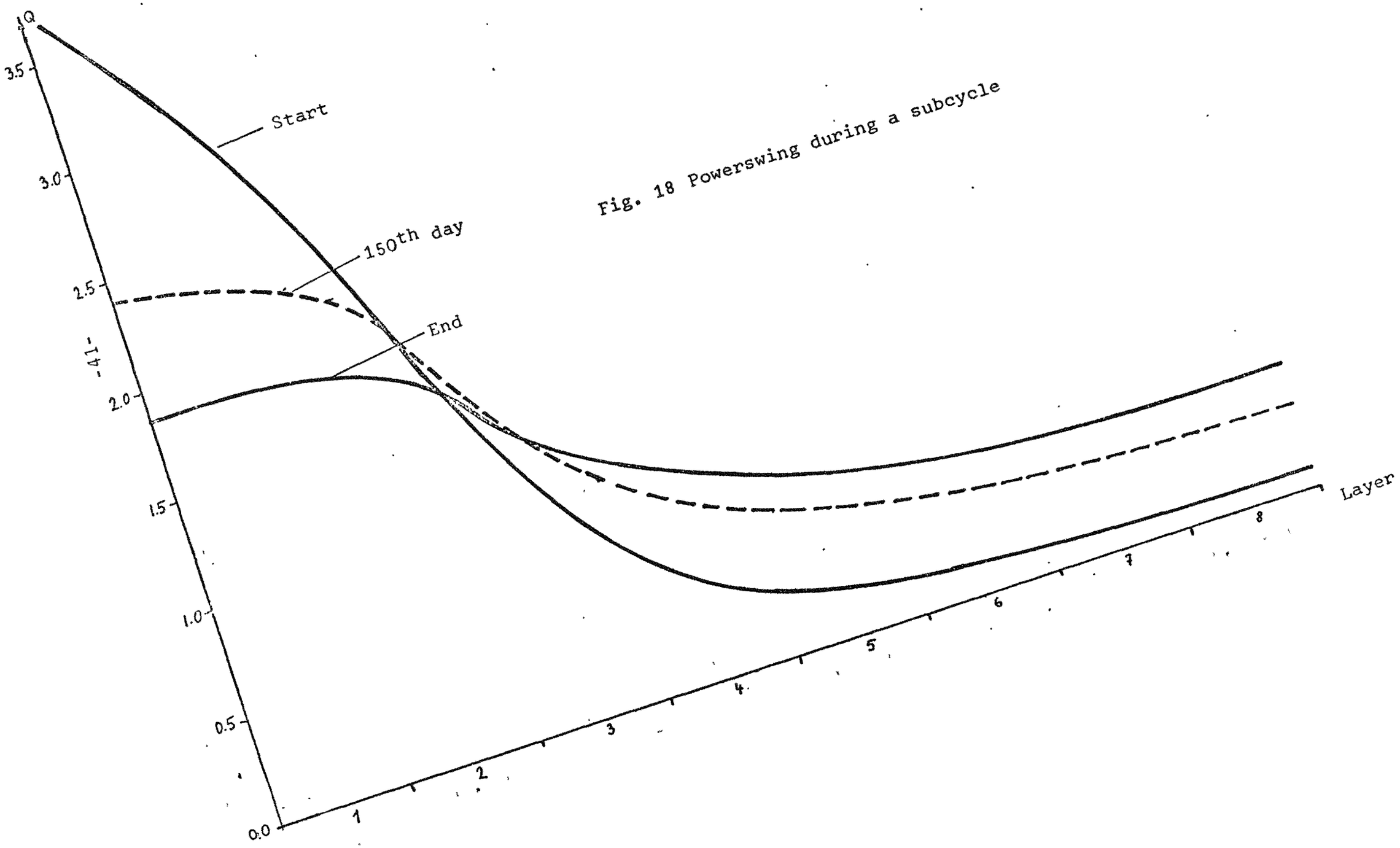

Fig. 18 Powerswing during a subcycle

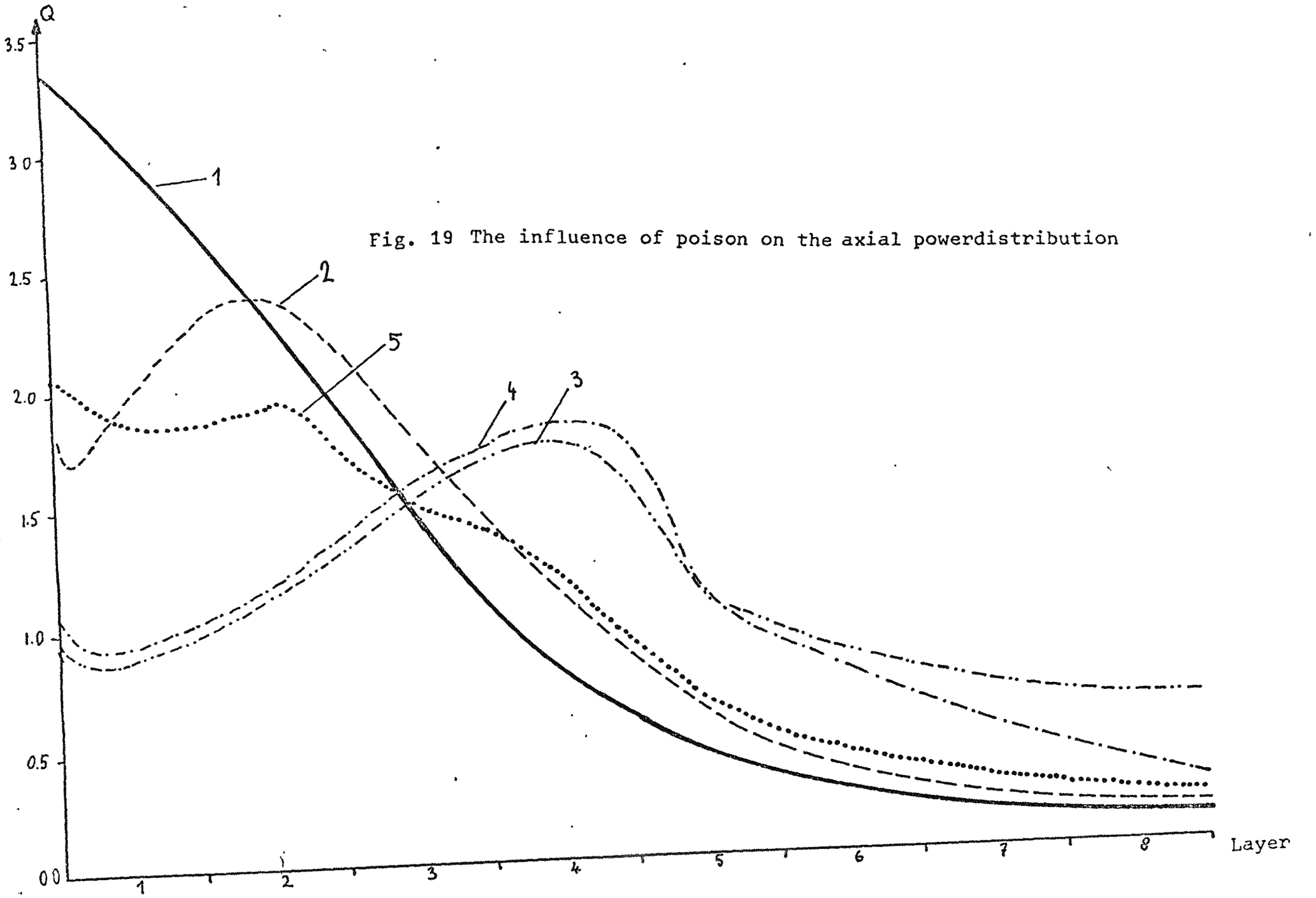

Fig. 19 The influence of poison on the axial powerdistribution

Fig:20 fast Dose(> 0.1 MeV) v. time

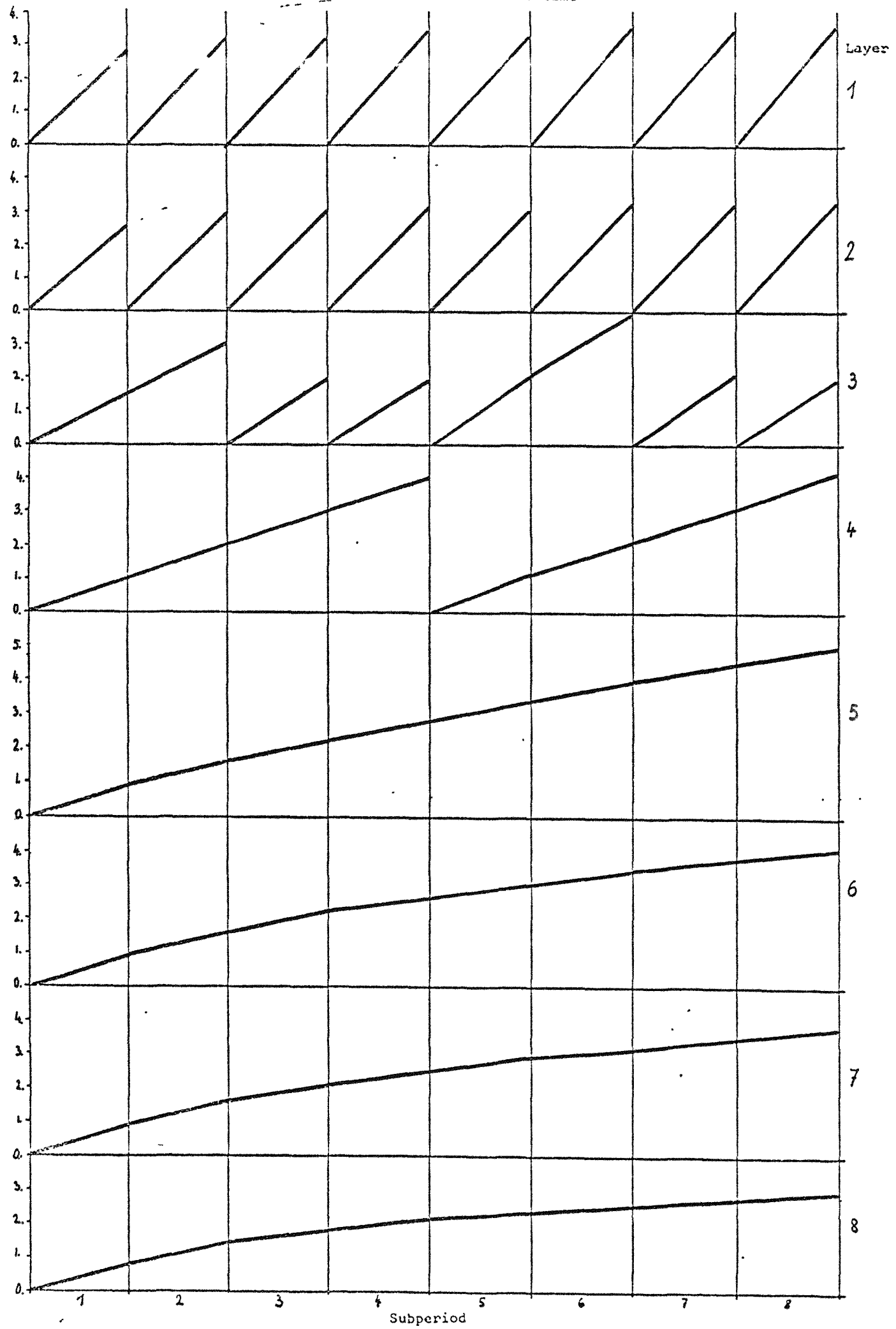

Fig:21 Fraktion of Fission from U-233
(normalised to 100%)